JOURNAL OF GEOPHYSICAL RESEARCH, VOL. 102, NO. B12, PAGES 27,729–27,749, DECEMBER 10, 1997

Origin of gabbro sills in the Moho transition zone of the Oman ophiolite: Implications for magma transport in the oceanic lower crust

Jun Korenaga[1] and Peter B. Kelemen

Department of Geology and Geophysics, Woods Hole Oceanographic Institution, Woods Hole, Massachusetts

Abstract. The Moho transition zone (MTZ) of the Oman ophiolite commonly includes a number of gabbro sills surrounded by dunites. The petrology and geochemistry of these sills are investigated to provide constraints on how magma migrates from the subridge mantle to the oceanic crust. The gabbro sills have millimeter-scale to tens of centimeter-scale modal layering that closely resembles layering in lower crustal gabbros of the ophiolite. Variations in mineral compositions correlate with the modal layering, but there are no overall trends within the sills. The gabbroic sills and the layered gabbros have clear covariations among mineral compositions, which can be interpreted as a fractional crystallization path from a common parental magma. Together with constraints from mid-ocean ridge thermal evolution and crustal accretion dynamics, the petrological and geochemical observations on the gabbro sills indicate that they formed from small, open-system, melt-filled lenses within the MTZ. The thermal evolution of the MTZ melt lenses, buffered by the ambient mantle, is characterized by a slow cooling rate ($<10^{-3}$°C/yr) and a small temperature difference (~0.1-1°C) within lenses. Internal origins for modal layering, such as gravity currents and oscillatory nucleation, are unlikely in such a thermal environment, and we propose that open-system evolution of the melt lenses is essential to produce the observed layering. The formation of the MTZ melt lenses may be a consequence of porous flow with low Peclet number entering a conductively cooling regime, where porosity becomes "clogged" by crystallized plagioclase. Preservation of fine-scale vertical variation in mineral composition, together with correlated compositions of different minerals, rules out diffuse porous flow as the primary mechanism of melt transport above these melt lenses. Instead, melt extraction must have been focused into porous channels or melt-filled fractures. Melt lenses drained by fractures would experience repetitious expulsion with continuous melt replenishment. Modal layering could develop through the expulsion cycles, probably via in situ crystallization at the margins of melt lenses.

1. Introduction

Understanding the magmatic construction of oceanic crust is essential for the study of chemical differentiation of primary magmas at mid-ocean ridges. Primary magma crossing the Moho from the mantle is modified during its ascent to the surface, and its differentiation within the crust can be complex, involving interaction with preexisting crustal components. On the basis of ophiolite studies, dredging, drilling, and seismic results, the oceanic crust is thought to be composed of lavas; sheeted dikes; upper, "isotropic" gabbros; and lower, layered gabbros. Models of a large-scale magma chamber that extends from beneath the sheeted dikes to the Moho and has a lateral dimension of >20 km were originally proposed to explain this crustal stratigraphy [e.g., *Cann*, 1974; *Pallister and Hopson*, 1981]; in this view, lavas and dikes are extruded from the magma chamber, whereas gabbros are crystallized along its margins.

Recent seismic experiments at present-day ridge axes have revealed a small-scale, midcrustal, axial melt lens underlain by low-velocity transition and mush zones at fast spreading ridges [e.g., *Detrick et al.*, 1987; *Harding et al.*, 1989; *Toomey et al.*, 1990]. The observed size of the melt lens, which is typically 1-2 km wide and 20-100 m thick [*Kent et al.*, 1990], led to a new view of the crustal construction processes. While lavas and dikes are products of episodic eruptions, the lower crustal layered gabbros are thought by some authors to be products of crystal fractionation in the midcrustal melt lens, transported to the lower crust by ductile flow [*Nicolas et al.*, 1988; *Phipps Morgan and Chen*, 1993; *Henstock et al.*, 1993; *Quick and Denlinger*, 1993]. Accordingly, more complex models of the geochemical evolution of mid-ocean ridge basalt (MORB) have been proposed, such as in situ differentiation within the lower crust [e.g., *Sinton and Detrick*, 1992].

[1]Also at Massachusetts Institute of Technology/Woods Hole Oceanographic Institution Joint Program, Cambridge, Massachusetts.

Paper number 97JB02604.
0148-0227/97/97JB-02604$09.00

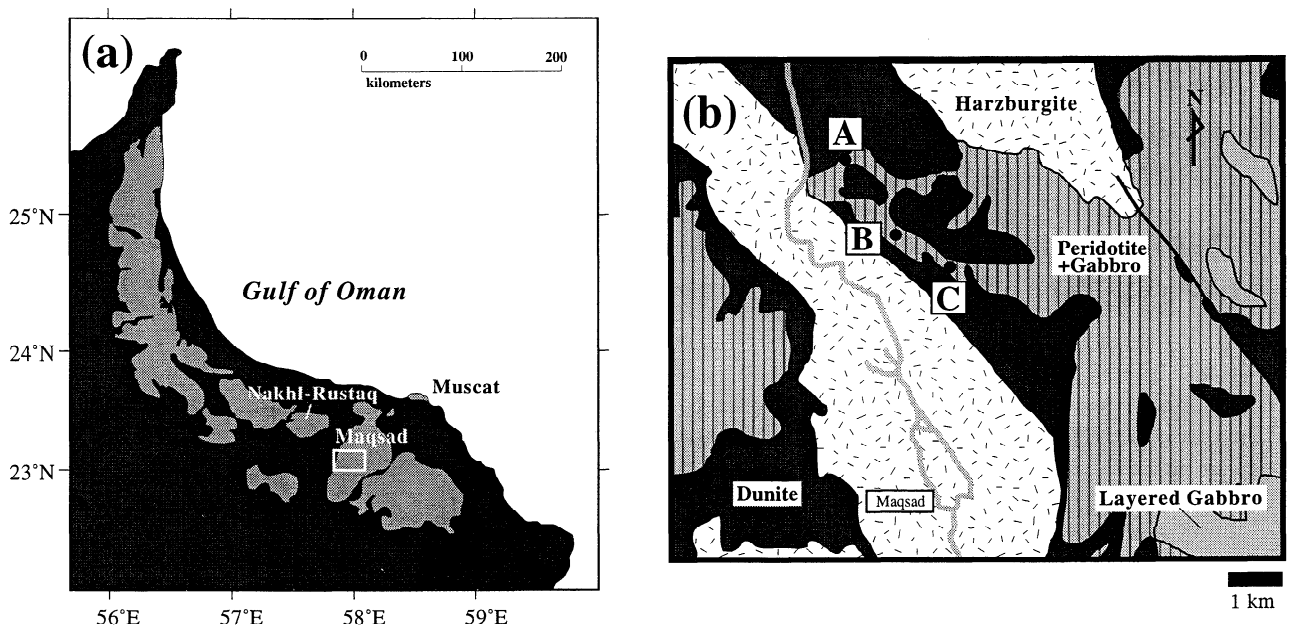

Figure 1. (a) The Oman ophiolite located at the southeastern corner of the Arabian peninsula. Gray shaded areas are exposed ophiolite massifs. Rectangle denotes the extent of Figure 1b. (b) Geologic map of the Maqsad area, based on geologic maps made by the French Bureau de Récherches Géologiques et Miniéres for the Sultanate of Oman. Gray stippled line denotes road, and solid line running northwest denotes major fault. Sample locations are shown by solid circles labeled A (Wadi Hajar), B (Wadi west of Tuf) and C (Tuf).

Magmatic evolution during ascent through the lower crust must be related to the processes of magma transport. Although some authors have suggested melt transport by porous flow within the transition and mush zones [e.g., *Quick and Denlinger*, 1993], porous flow is inconsistent with the cryptic variations observed in the layered gabbros of the Oman ophiolite. Cryptic or compositional variations are variations in mineral chemistry such as the forsterite (Fo) content in olivine. In the Oman ophiolite, there is a good correlation between compositional variations in olivine, clinopyroxene, and plagioclase [*Pallister and Knight*, 1981; *Browning*, 1984]. If porous flow were a dominant transport mechanism, these cryptic variations would have migrated at different velocities [e.g., *Irvine*, 1980; *McKenzie*, 1984; *Korenaga and Kelemen*, 1997], and no correlation of different species would be observed. Although a very small contribution of porous flow (less than a few percent of the total incoming melt flux) is not precluded [*Korenaga and Kelemen*, 1997], it cannot be the main mode of melt supply from the mantle to form the upper oceanic crust. Instead, focused melt transport, such as flow in cracks, is required. Gabbroic sills are common in the Moho transition zone of the Oman ophiolite [*Benn et al.*, 1988; *Boudier and Nicolas*, 1995; *Boudier et al.*, 1996]. *Kelemen et al.* [1997a] proposed that gabbroic sills are relicts of small, melt-filled lenses in the Moho transition zone (MTZ) and that accumulation of melt in the MTZ melt lenses may have been a source of overpressure to trigger the formation of melt-filled fractures.

Interpretations of the gabbro sills in the MTZ include (1) melt pockets resulting from porous flow processes during corner flow in the mantle [*Rabinowicz et al.*, 1987; *Boudier and Nicolas*, 1995], (2) lateral fractures associated with stress field rotation [*Ildefonse et al.*, 1993], and (3) liquid ponds formed beneath low permeability barriers [*Kelemen et al.*, 1997a]. Each of these models has different implications for the significance of the sills in the evolution of MORB. The purpose of this paper is to investigate the origin of the gabbro sills using their petrology and geochemistry to understand their possible role in the magmatic construction of the oceanic crust, particularly at fast spreading ridges.

2. Geological Setting

The Oman ophiolite consists of fragments of oceanic lithosphere, formed in the Tethys ocean 95-100 m.y. ago and then obducted onto the eastern Arabian margin 15 m.y. later [*Tilton et al.*, 1981; *Montigny et al.*, 1988]. The ophiolite constitutes the major part of the 700-km-long arcuate chain of the Oman Mountains (Figure 1) and is one of the largest ophiolite complexes in the world. The complete ophiolite sequence, i.e., volcanic rocks, sheeted dikes, gabbroic rocks, and ultramafic complexes [*Geotimes*, 1972], can be identified in many of the Oman massifs [e.g., *Coleman and Hopson*, 1981; *Lippard et al.*, 1986; *Nicolas*, 1989]. A continuous layer of sheeted dikes, as well as radiolarian cherts overlying the volcanic rocks, is consistent with crustal formation at an oceanic spreading center. In detail, however, the rare Earth elements (REEs) and other incompatible trace elements have lower concentrations at a given Cr concentration than most MORBs [e.g., *Pearce et al.*, 1981; *Alabaster et al.*, 1982]. Also, in some of the northern massifs, andesitic lavas make up part of the extrusive section. These characteristics suggest that the ophiolite may have formed in a suprasubduction zone setting. However, strong similarities between the com-

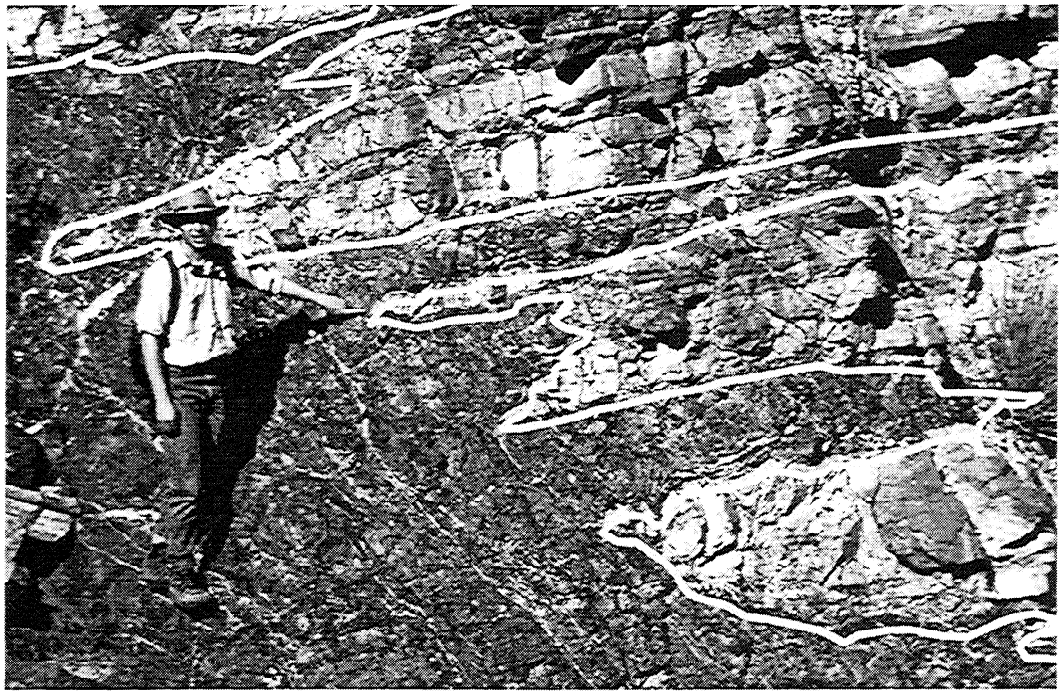

Figure 2. Photograph of layered gabbro sills in NW Wadi Tuf, intruding dunite in the Moho transition zone of the Maqsad area, Oman ophiolite. White outline emphasizes commonly observed, interfingering contact relationships between layered gabbro and dunite.

positions of Oman lavas, in general, and MORB are compelling evidence that petrogenetic processes in the ophiolite were similar to these operating at a normal mid-ocean ridge. Because uranium-lead radiometric dating and geological relations indicate that the ophiolite was originally formed at a fast spreading ridge [*Tilton et al.*, 1981; *Nicolas*, 1989], we concentrate on crustal genesis at fast spreading ridges in this paper.

A distinct complex called the crust/mantle transition zone or MTZ has been identified at the transition from overlying gabbroic (>95% gabbro over vertical distances >10 m) to underlying ultramafic (>95% residual peridotite and dunite over vertical distances >10 m) complexes [e.g., *Nicolas and Prinzhofer*, 1983; *Benn et al.*, 1988; *Boudier and Nicolas*, 1995]. The thickness of the MTZ varies from a few hundred to tens of meters. In contrast to the underlying mantle section, composed mainly of harzburgite, the MTZ is composed predominantly of dunite and gabbro. Gabbros in the MTZ commonly form sills intruding dunite (Figure 2). Sill thicknesses vary from ~1 m to tens of meters. The horizontal extent of the sills ranges from ten to a few hundred meters, and their aspect ratios are generally larger than 10 [*Boudier et al.*, 1996]. The contact between the gabbro sills and the surrounding dunitic rocks is either diffuse or sharp, and no chilled margins are observed. The sills have a millimeter-scale to tens of centimeter-scale modal layering, which closely resembles the modal layering observed in the lower crustal layered gabbros. The number of sills generally increases upward in the MTZ, and the resultant dunite/gabbro interlayering makes a smooth transition to the layered gabbroic complex above the MTZ. For the purpose of discussion, the (petrologic) Moho is defined here as the base of the continuous layered gabbro section [*Benn et al.*, 1988].

An essential caveat is that, in addition to features emplaced "on-axis" beneath a submarine spreading ridge, ophiolites also preserve features formed "off-axis" in the oceanic lithosphere. In the case of the Oman ophiolite, igneous ages and emplacement ages are virtually the same, within error (B. Hacker, personal communication, 1995, and summaries by *Boudier et al.* [1985] and *Michard et al.* [1991]), so that on-axis structures may have been affected by the emplacement process and by unusually rapid cooling as the ridge system ceased to be active. For these reasons, one might question whether gabbroic sills in the MTZ in Oman resemble steady state features beneath a normal mid-ocean ridge.

We believe, however, that sills along the MTZ are, in fact, characteristic of normal fast spreading ridges for the following reasons. (1) Major and trace element geochemistry of the gabbroic sills indicates that their constituent minerals are in exchange equilibrium with the liquids that formed the sheeted dikes and lavas of the ophiolite [*Kelemen et al.*, 1997a]. This is also true of minerals in the lower crustal gabbros [*Pallister and Hopson*, 1981; *Kelemen et al.*, 1997a]. Mass balance requires that the liquid extracted from gabbroic sills in the MTZ and from lower crustal gabbros must make up a substantial proportion of the crust. Thus, the liquids extracted from the sills and lower gabbros must be represented by the sheeted dikes and overlying lavas; all must have formed at a spreading ridge. (2) The MTZ must be at or above the level of plagioclase (and clinopyroxene) saturation in ascending magmas at fast spreading ridges. Thus it is reasonable that gabbroic rocks should become abundant within the MTZ on axis. (3) Seismic data suggest high melt proportions near the

Table 1. Petrography of OM95 and OM96 Gabbros

Sample[a]	Rock Type	Primary Mode[b]				Secondary Minerals,[c]	Location[d]
		Ol	Pl	Cpx	Opq	%	
95-40A	mela troctolite	73.8	20.6	3.1	2.4	30 serp, pr, hbl	A[e]
95-40B	mela troctolite	69.7	26.5	2.5	1.3	40 serp, pr	A[e]
95-41A	olivine gabbro	39.1	34.2	26.3	0.4	20 serp, pr	A[f]
95-41B	olivine gabbro	43.8	34.0	21.7	0.5	18 serp, pr	A[f]
95-42A	olivine gabbro	21.6	46.3	32.0		27 pr, serp	A[g]
95-42B	olivine gabbro	32.4	38.5	28.6	0.5	31 pr, serp	A[g]
95-P12	olivine gabbro	28.5	38.9	32.5	0.1	37 pr, serp	B
95-P13	olivine gabbro	33.1	43.2	23.2	0.5	15 serp, pr	B
96-44A	olivine gabbro	19.1	51.5	29.4	0.1	23 pr, serp	C[h]
96-44B	olivine gabbro	35.5	38.9	25.6	0.1	28 serp, pr	C[h]
96-44C	olivine gabbro	37.3	33.9	28.7	0.1	23 serp, pr	C[h]
96-49A	olivine gabbro	21.8	39.2	38.6	0.3	20 serp, pr, hbl	C[h]
96-49B	olivine gabbro	18.7	43.0	38.2	0.1	20 serp, pr	C[h]
96-49C	olivine gabbro	25.8	43.7	30.4	0.1	12 pr, serp	C[h]
96-54A	olivine gabbro	27.2	31.4	41.3	0.1	27 pr, serp	C[h]
96-54B	olivine gabbro	31.3	40.4	28.1	0.2	25 serp, pr	C[h]
96-67A	olivine gabbro	40.2	35.6	24.2		55 pr, serp	B
96-67B	olivine gabbro	38.1	35.4	26.4		57 pr, serp	B
96-67C	olivine gabbro	45.4	33.5	21.1	0.1	52 serp, pr	B
96-68A	olivine gabbro	28.0	42.5	29.4	0.1	53 pr, serp	B
96-68B	olivine gabbro	29.8	43.3	27.0		65 pr, serp	B
96-71	olivine gabbro	23.1	39.6	37.4		35 pr, serp	B[i]
96-73	olivine gabbro	19.1	45.8	34.9	0.2	23 pr, serp, hbl	B[i]
96-74	olivine gabbro	32.9	35.9	31.1	0.1	28 pr, serp, hbl	B[i]
96-76A	olivine gabbro	18.0	41.6	40.0	0.3	29 pr, serp, hbl	B[i]
96-76B	olivine gabbro	22.1	50.2	27.6	0.2	31 pr, serp, hbl	B[i]

[a]Sample pairs (e.g.,40A and 40B) represent subsamples of individual rocks.

[b]Estimated primary mode includes pseudomorphs. Abbreviations are Ol,olivine; Pl,plagioclase; Cpx,Clinopyroxene; Opq,opaques.

[c]Percentages give total modal percent of secondary minerals. Abbreviations are serp,serpentinite; pr,prehnite; hbl,hornblende.

[d]A, B, and C denote Wadi Hajar, Wadi west of Tuf, and Tuf, respectively.

[e]Locale is 50 m below the Moho.

[f]Locale is ~20 m above sample 95-40.

[g]Locale is ~20 m above sample 95-41.

[h]Locale is a continuous gabbroic section with different distances to its base; 44 is 1.37 m, 49 is 0.98 m, and 54 is 2.49 m.

[i]Locale is a continuous gabbroic section with different distances to its base; 71 is 0.11 m, 73 is 1.01 m, 74 is 2.17 m, and 76 is 3.45 m.

MTZ beneath active spreading ridges [*Dunn et al.*, 1994; W. C. Crawford et al., submitted to Nature, 1996]. Thus there is evidence for accumulation of melt near the MTZ at fast spreading, mid-ocean ridges. In later sections, we discuss whether the present study is consistent with our hypothesis that sills form on axis in the MTZ at fast spreading ridges and are an important component of the crustal accretion process.

3. Petrology and Geochemistry of Gabbro Sills

The rock samples analyzed in this work were collected from the MTZ of the Maqsad massif during 1995 and 1996 field excursions, in cooperation with a French team led by A. Nicolas and F. Boudier. The Maqsad area (Figure 1) is well suited for our reconnaissance investigation of the gabbro sills because the Moho is almost flat lying and a thick (~500 m) MTZ is exposed. This massif is a well-studied region within the Oman ophiolite; detailed geological maps of this area have been published by *Boudier and Nicolas* [1995] and *Ceuleneer et al.* [1996]. Several well-preserved gabbro sills were selected at three main sampling locations in the area (Figure 1b). Some sills more than a few meters thick were multiply sampled from the base to the top, perpendicular to the Moho, to examine possible vertical heterogeneities.

3.1. Petrography

Modes determined on 26 gabbroic samples are shown in Table 1, with the description of sample locations. The primary mode includes pseudomorphs after primary minerals. On the basis of the modal analyses, rock types were determined following the recommended International Union of Geological Sciences classification scheme [*Streckeisen*, 1976]. Multiple thin sections were made of most rocks to cover at least one complete cycle of modal layering, and an average of 3800 points with a 2/3 mm spacing was counted for each sample.

The average size of olivine grains in the gabbroic rocks ranges from 1.0 to 2.0 mm, while the average size of plagioclase and clinopyroxene grains ranges from 1.5 to 2.5 mm. In the mela-troctolite sample (95-40), clinopyroxene is observed only as interstitial grains between plagioclase and olivine. Olivine grains are moderately serpentinized, and plagioclase shows various degrees of alteration to prehnite and hydrogrossular. Clinopyroxenes are generally least altered, only locally showing replacement by amphiboles. Most grains are idiomorphic to hypidiomorphic, though poikilitic textures are also locally observed; small (~0.3 mm) olivine grains are commonly included in larger clinopyroxenes and plagioclases. Modal layering is common; the scale of layering is typically a few centimeters, and various styles in modal layering have been identified. Variations in the modal proportion of olivine and plagioclase are generally more prominent than that of clinopyroxene. Transitions from olivine-rich, melanocratic layers to plagioclase-rich, leucocratic layers are both gradational and sharp. The gradational changes from melanocratic to leucocratic bands are generally "normally" graded, i.e., showing gradational increase in the plagioclase proportion upward with a sharp change at the top of a graded layer from plagioclase-rich to plagioclase-poor lithologies. Some samples are, however, "reversely" graded.

3.2. Mineral chemistry

Electron microprobe analyses. Compositions of primary minerals were measured using the JEOL 733 electron microprobe at Massachusetts Institute of Technology, with 15-keV accelerating voltage and 10-nA beam current (Tables 2-4). The focused beam diameter was 1 μm for olivine and clinopyroxene and 10 μm for plagioclase, and counting times were 20-40 s, depending on elements. Data were reduced using the *Bence and Albee* [1968] matrix correction scheme as modified by *Albee and Ray* [1970]. Analytical errors are estimated as <2% relative for major element concentrations and >15% relative for trace element concentrations. To detect possible correlations between modal layering and mineral chemistry, measurements of grain cores were conducted at approximately 5-mm intervals along the vertical axis. Several grain rims were analyzed to examine compositional zoning, and when there were vertical compositional variations, several grains at the same levels were analyzed to check for lateral heterogeneities.

No significant zoning was observed in any of the primary minerals; intragrain heterogeneities are mostly comparable with analytical errors. Olivine Mg numbers, defined as molar Mg/(Mg+Fe) × 100 , with Fe equal to total iron, range from 80.4 to 88.7 (Table 2). Plagioclases are highly calcic, with average compositions ranging from $An_{85.4}$ to $An_{90.7}$ (Table 3). Clinopyroxene Mg numbers, ranging from 84.6 to 91.9 (Table 4), show a sympathetic variation with the Mg numbers of coexisting olivines (Figure 3). The correlation in the Mg numbers of the coexisting olivines and clinopyroxenes is in good agreement with the equilibrium Fe-Mg partition coefficients determined from one-atmosphere experiments; that is, $K_D^{Ol/liq} = 0.29$ and $K_D^{Cpx/liq} = 0.23$ [*Walker et al.*, 1979; *Grove and Bryan*, 1983].

Table 2. Average Compositions of Olivine

Sample	N^a	SiO_2	Al_2O_3	FeO	MgO	CaO	TiO_2	Cr_2O_3	MnO	NiO	Total	Mg#[b]
95-40A	8	39.8	0.0	10.9	48.2	0.1	0.0	0.0	0.2	0.3	99.5	88.7(0.2)
95-40B	8	39.9	0.1	11.0	48.4	0.1	0.0	0.1	0.2	0.3	100.0	88.7(0.1)
95-41A	28	39.3	0.0	15.4	45.5	0.0	0.0	0.0	0.2	0.2	100.8	84.0(0.3)
95-41B	20	39.6	0.0	14.9	45.7	0.0	0.0	0.0	0.2	0.2	100.7	84.5(0.3)
95-42A	14	39.8	0.0	12.5	47.0	0.0	0.0	0.0	0.2	0.2	99.7	87.0(0.3)
95-42B	21	39.9	0.0	12.5	47.2	0.0	0.0	0.0	0.2	0.2	100.0	87.1(0.2)
95-P12	12	39.1	0.0	16.5	43.9	0.0	0.0	0.0	0.2	0.1	100.0	82.5(0.5)
95-P13	25	39.3	0.0	13.9	46.1	0.0	0.0	0.0	0.2	0.2	99.7	85.6(0.6)
96-44A	10	39.0	0.0	17.6	43.9	0.0	0.0	0.0	0.3	0.1	100.9	81.7(0.4)
96-44B	11	39.3	0.0	17.0	44.0	0.0	0.0	0.0	0.2	0.2	100.8	82.1(0.3)
96-44C	12	39.2	0.1	16.8	44.3	0.0	0.0	0.1	0.3	0.2	100.9	82.4(0.3)
96-49A	11	38.9	0.0	18.7	43.1	0.0	0.0	0.0	0.2	0.2	101.0	80.4(0.4)
96-49B	12	38.6	0.1	18.4	42.3	0.0	0.0	0.0	0.2	0.1	99.8	80.4(0.3)
96-49C	15	38.6	0.0	17.9	42.6	0.0	0.0	0.0	0.2	0.1	99.5	80.9(0.3)
96-54A	12	39.0	0.0	17.3	43.9	0.0	0.0	0.0	0.3	0.1	100.7	81.9(0.4)
96-54B	16	38.7	0.0	17.4	43.1	0.0	0.1	0.0	0.3	0.1	99.7	81.5(0.4)
96-67A	17	39.3	0.0	14.6	45.5	0.0	0.0	0.0	0.2	0.1	99.8	84.8(0.4)
96-67B	15	39.4	0.1	14.3	46.5	0.0	0.0	0.0	0.2	0.1	100.6	85.3(0.3)
96-67C	9	39.8	0.0	13.7	46.4	0.0	0.1	0.0	0.2	0.1	100.4	85.8(0.1)
96-68A	12	39.7	0.0	15.3	46.1	0.0	0.0	0.1	0.2	0.1	101.5	84.3(0.4)
96-68B	10	39.8	0.0	13.9	46.3	0.0	0.1	0.0	0.2	0.2	100.5	85.5(0.5)
96-71	12	39.2	0.1	15.0	45.2	0.0	0.0	0.0	0.2	0.2	99.9	84.3(0.3)
96-73	21	39.1	0.0	14.6	45.3	0.0	0.1	0.0	0.2	0.2	99.6	84.7(0.5)
96-74	22	39.2	0.1	15.3	44.9	0.1	0.0	0.0	0.2	0.1	99.9	83.9(0.5)
96-76A	18	39.1	0.0	15.3	44.9	0.0	0.0	0.0	0.1	0.2	99.7	83.9(0.3)
96-76B	15	39.2	0.0	15.1	45.4	0.0	0.0	0.0	0.2	0.3	100.2	84.3(0.4)

Values are in weight percent.
[a]Values indicate number of analyses.
[b]Mg# = molar Mg/(Mg+Fe) × 100, where Fe is total iron. One standard deviation is in parentheses.

Table 3. Average Compositions of Plagioclase

Sample	N^a	SiO_2	Al_2O_3	FeO	MgO	CaO	Na_2O	K_2O	Total	An^b
95-40A	6	45.1	33.9	0.1	0.0	18.5	1.0	0.0	98.7	90.7(0.5)
95-40B	6	45.0	34.0	0.1	0.1	18.3	1.1	0.0	98.6	90.5(0.4)
95-41A	16	45.8	34.4	0.3	0.0	18.2	1.3	0.0	100.1	88.4(0.7)
95-41B	11	46.2	34.7	0.3	0.0	18.2	1.3	0.0	100.7	88.2(0.4)
95-42A	16	45.5	34.4	0.2	0.0	18.2	1.2	0.0	99.6	89.7(0.7)
95-42B	19	45.5	34.8	0.2	0.0	18.4	1.1	0.0	100.1	90.2(1.1)
95-P12	11	46.2	34.2	0.2	0.0	17.8	1.5	0.0	99.8	87.0(0.7)
95-P13	17	45.4	33.5	0.2	0.0	17.9	1.3	0.0	98.4	88.1(0.5)
96-44A	20	45.9	34.8	0.2	0.0	18.1	1.3	0.0	100.3	88.3(0.7)
96-44B	11	45.8	34.4	0.1	0.1	18.2	1.2	0.0	99.9	89.3(0.9)
96-44C	11	45.7	34.1	0.2	0.0	18.2	1.2	0.0	99.5	89.3(0.9)
96-49A	11	45.8	35.2	0.2	0.0	18.4	1.2	0.0	100.7	89.5(0.5)
96-49B	13	45.3	33.9	0.2	0.0	18.1	1.2	0.0	98.6	89.5(0.7)
96-49C	16	45.3	33.7	0.2	0.1	18.0	1.2	0.0	98.6	89.2(0.6)
96-54A	11	45.7	35.1	0.2	0.0	18.5	1.2	0.0	100.7	89.8(0.7)
96-54B	19	45.2	33.9	0.2	0.0	18.2	1.1	0.0	98.7	90.0(0.8)
96-67A	3	46.9	35.2	0.1	0.0	17.6	1.6	0.0	101.5	85.6(0.7)
96-67B	8	46.9	34.8	0.2	0.0	17.6	1.6	0.0	101.2	85.8(0.2)
96-67C	8	46.4	33.3	0.2	0.0	17.5	1.7	0.0	99.1	85.4(0.5)
96-68A	8	46.7	33.6	0.2	0.0	17.6	1.6	0.0	99.9	85.6(0.8)
96-68B	5	46.6	33.6	0.2	0.0	17.6	1.6	0.0	99.6	85.9(0.1)
96-71	15	45.2	33.8	0.2	0.1	18.2	1.2	0.0	98.7	89.7(0.6)
96-73	17	45.2	33.7	0.2	0.0	18.1	1.2	0.0	98.5	89.3(0.5)
96-74	21	45.3	33.8	0.2	0.1	18.1	1.2	0.0	98.6	89.5(0.7)
96-76A	21	45.4	33.9	0.2	0.0	18.1	1.2	0.0	98.9	89.1(0.4)
96-76B	12	45.3	35.1	0.2	0.0	18.0	1.2	0.0	99.8	89.1(0.4)

Values are in weight percent.
[a]Values indicate number of analyses.
[b]Numbers in parentheses represent 1 standard deviation.

Table 4. Average Compositions of Clinopyroxene

Sample	N^a	SiO_2	Al_2O_3	FeO*	MgO	CaO	Na_2O	TiO_2	Cr_2O_3	MnO	Total	Wo^b	En^b	Fs^b	$Mg\#^c$
95-40A	9	52.3	3.1	2.7	16.5	24.3	0.3	0.2	0.8	0.1	100.3	49.2	46.5	4.3	91.5(1.2)
95-40B	10	52.0	3.2	2.5	16.2	24.6	0.3	0.4	0.8	0.1	100.1	50.1	45.9	4.0	91.9(1.0)
95-41A	31	51.8	3.5	4.3	16.8	22.6	0.2	0.3	0.6	0.1	100.3	45.7	47.5	6.8	87.4(0.6)
95-41B	29	51.9	3.6	4.4	17.0	22.4	0.3	0.3	0.7	0.1	100.7	45.3	47.7	6.9	87.3(0.5)
95-42A	21	52.5	3.2	3.9	17.8	22.0	0.2	0.4	0.5	0.1	100.4	44.2	49.7	6.1	89.2(0.7)
95-42B	35	52.5	3.2	3.7	17.4	22.5	0.2	0.3	0.5	0.1	100.4	45.4	48.8	5.8	89.4(0.8)
95-P12	14	51.9	3.3	4.9	16.6	22.3	0.3	0.4	0.5	0.1	100.4	45.4	46.9	7.7	85.9(1.1)
95-P13	41	51.5	3.6	4.1	16.7	22.5	0.3	0.3	0.6	0.1	99.6	46.0	47.5	6.5	88.0(0.7)
96-44A	12	51.9	3.5	4.4	16.2	23.0	0.3	0.3	0.4	0.1	100.3	46.9	46.1	7.0	86.8(0.7)
96-44B	17	51.7	3.7	4.8	16.4	22.7	0.2	0.4	0.5	0.0	100.4	46.1	46.4	7.5	86.0(0.8)
96-44C	17	51.8	3.6	4.7	16.5	22.9	0.2	0.3	0.5	0.1	100.7	46.2	46.4	7.4	86.3(0.6)
96-49A	21	51.9	3.7	5.4	16.4	22.0	0.2	0.3	0.4	0.1	100.4	44.8	46.6	8.6	84.6(1.2)
96-49B	46	51.2	3.5	5.1	16.3	22.2	0.2	0.3	0.4	0.2	99.5	45.4	46.4	8.2	85.0(0.7)
96-49C	16	51.2	3.3	4.9	16.3	22.5	0.2	0.3	0.3	0.1	99.2	45.8	46.3	7.8	85.5(0.6)
96-54A	12	51.9	3.6	5.3	17.0	21.5	0.2	0.3	0.5	0.1	100.3	43.6	48.0	8.3	85.3(1.7)
96-54B	28	51.1	3.8	4.5	16.3	22.4	0.3	0.4	0.5	0.1	99.4	46.2	46.6	7.2	86.7(1.1)
96-67A	19	52.6	3.2	4.7	17.5	21.7	0.3	0.4	0.6	0.1	101.1	43.7	49.0	7.3	87.0(0.8)
96-67B	10	52.6	3.2	4.2	17.0	22.4	0.3	0.4	0.6	0.1	100.6	45.4	47.9	6.7	87.7(0.6)
96-67C	10	52.2	3.7	4.3	17.3	21.8	0.3	0.4	0.7	0.1	100.8	44.3	48.9	6.8	87.8(0.8)
96-68A	9	52.5	3.5	4.4	16.9	22.7	0.3	0.3	0.5	0.1	101.2	45.8	47.3	7.0	87.2(0.3)
96-68B	11	52.4	3.7	4.3	17.2	21.8	0.3	0.4	0.8	0.1	101.0	44.4	48.7	6.9	87.6(0.7)
96-71	19	51.4	3.5	4.3	16.9	22.3	0.2	0.3	0.6	0.1	99.6	45.4	47.8	6.8	87.5(0.6)
96-73	41	51.4	3.5	4.2	16.9	22.3	0.2	0.3	0.6	0.1	99.5	45.4	47.9	6.7	87.8(0.5)
96-74	21	51.3	3.4	4.3	16.7	22.4	0.2	0.4	0.7	0.1	99.5	45.6	47.5	6.9	87.4(0.5)
96-76A	19	51.7	3.4	4.6	17.0	22.0	0.2	0.3	0.6	0.1	99.8	44.6	48.2	7.3	87.0(1.0)
96-76B	20	51.6	3.6	4.5	17.1	22.0	0.2	0.4	0.8	0.1	100.2	44.6	48.2	7.1	87.2(0.8)

Values are in weight percent.
[a]Values denote number of analyses.
[b]Values denote molar proportions in normative minerals. Abbreviations are Wo,wollastonite; En,enstatite; and Fs,ferrosilite.
[c]Mg# = molar Mg/(Mg+Fe) × 100, where Fe is total iron. One standard deviation is in parentheses.

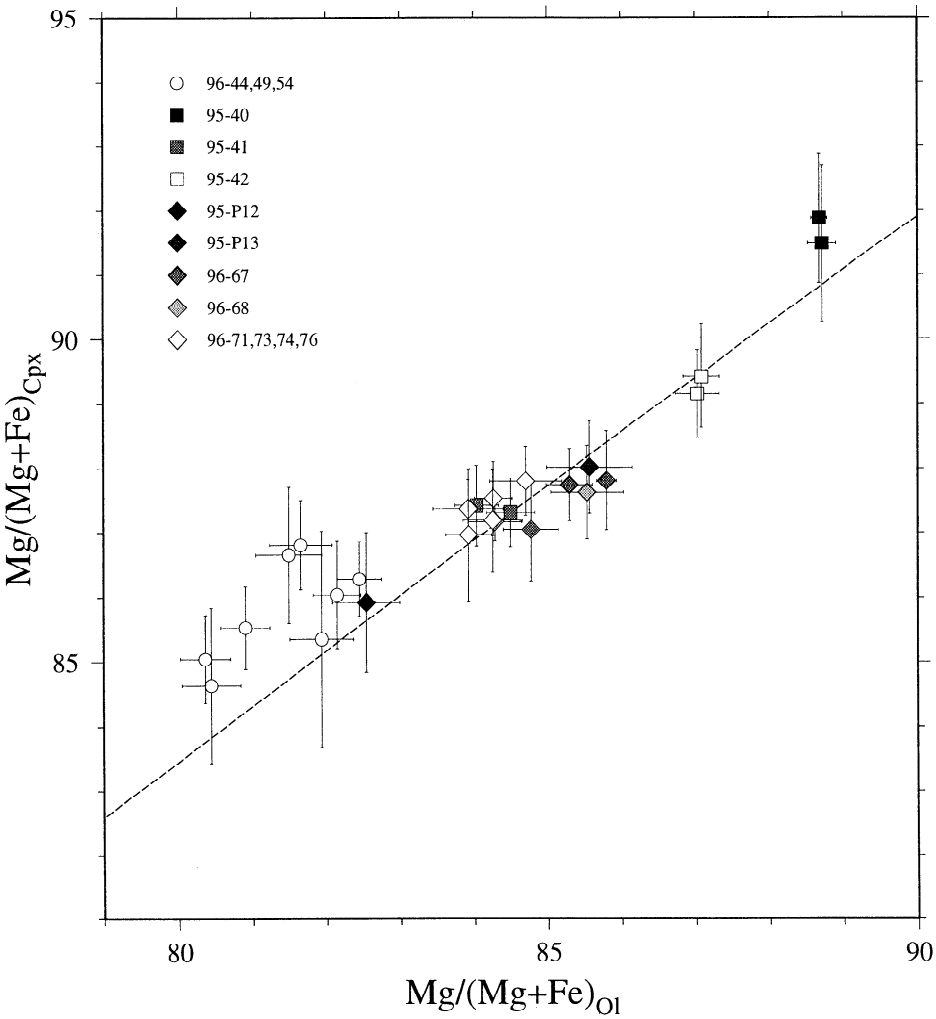

Figure 3. Olivine Mg numbers plotted with coexisting clinopyroxene Mg numbers. Data are averaged per sample, and error bars denote 1 standard deviation. Predicted correlation based on partition coefficient $K_D^{\mathrm{Ol/liq}} = 0.29$ and $K_D^{\mathrm{Cpx/liq}} = 0.23$ is shown as a dashed line.

Compositional variations occur on the scale of a few centimeters for the Fo content of olivines and the Cr_2O_3 content of clinopyroxenes (Figure 4). The compositional variations correlate moderately well with modal layering; the Fo and Cr_2O_3 contents generally decrease as the modal proportion of olivine decreases. The compositional variations appear to depend on the compatibility of the individual elements; incompatible chemical species, such as TiO_2 in clinopyroxenes, show almost constant values within samples (Figure 4). The An content of plagioclase also lacks systematic variation. The NiO and MnO contents of olivines are rather scattered, with larger intragrain and lateral heterogeneities and larger analytical errors, so it is hard to interpret any trend in these data. Apart from the above small-scale compositional variations in the Fo and Cr_2O_3 contents within individual layers, there is no overall trend in mineral compositions within the sills (Figure 4).

Ion microprobe analyses. To confirm the dependence of compositional variations, trace element concentrations in clinopyroxenes were measured using the Cameca IMS/3F secondary mass spectrometer at Woods Hole Oceanographic Institution (Table 5). The analytical method for ion probe analysis is described by *Shimizu and Hart* [1982]. A primary beam of ~15 nA, focused to a spot of ~20 μm, was used to analyze clinopyroxene cores, at an approximately 1 cm interval. Estimated errors of measurement are <10% relative to the concentrations. Clinopyroxenes in sample 95-40 were not analyzed because they are interstitial grains that are too small for ion probe analysis.

Good agreement is achieved between electron probe and ion probe analyses of Cr in clinopyroxene (Figure 4). Despite a systematic offset in concentration, the ion probe and electron probe data consistently indicate no systematic variation in the TiO_2 content with height. Zr, another moderately incompatible element, also lacks compositional variation.

3.3. Geochemical Relationship Between Gabbro Sills and Lower Crustal Gabbros

Covariations of mineral compositions in the gabbro sills in the Maqsad area are plotted in Figure 5, together with data from gabbroic rocks in the adjacent Rustaq area reported by *Browning* [1982]. The geochemistry of the gabbroic rocks in the Rustaq MTZ is very similar to that of the gabbro sills in this study. MTZ gabbros from Maqsad and Rustaq define the primitive end of continuous geochemical trends with the lower crustal, layered gabbros in Rustaq. The observed co-

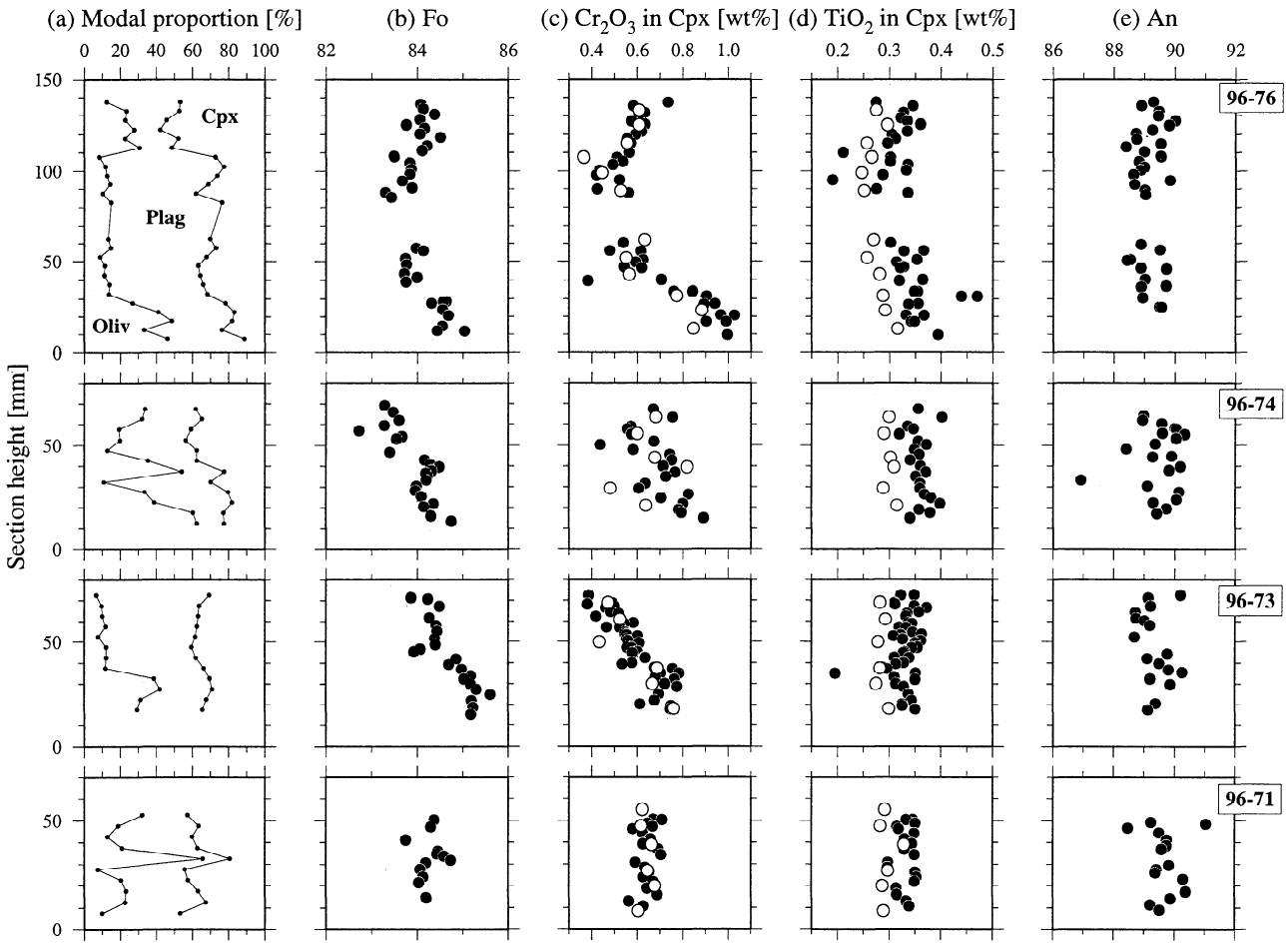

Figure 4. An example of fine-scale mineral chemistry analyses. (a) Modal proportions, (b) Fo content of olivine, (c) Cr_2O_3 and (d) TiO_2 contents of clinopyroxene, and (e) An content of plagioclase. Open circles in Figures 4c and 4d denote ion probe analyses. These four samples were taken from the same sill (Table 1), and data are displayed to reflect actual stratigraphic relations.

variations suggest fractional crystallization paths for similar parental liquids. The previously noted lack of clear trends in incompatible element concentrations may be explained by the small degree of differentiation within the MTZ; incompatible elements are only slightly concentrated during the initial stage of differentiation, whereas compatible elements are rapidly extracted from the liquid by crystallization [e.g., *McBirney*, 1993, Figure 5-22]. The lower crustal gabbros have limited ranges of compatible element abundances and more drastic variations in incompatible element contents, consistent with the interpretation that they represent products of more extensive differentiation from similar parental liquids.

4. Crystallization Processes in On-Axis, Small-Scale MTZ Melt Lenses

The mineral chemistry of the MTZ gabbros falls in distinct chemical fields, showing little overlap with lower crustal gabbros. The Fo content of the MTZ gabbros is generally greater than 80, while that of the lower crustal gabbros is mostly less than 80. Considering that olivines in equilibrium with mantle-derived melts would have a Fo content of ~90 and considering the scarcity of incompatible elements in the lower crustal gabbros (little or no trapped liquid [e.g., *Pallister and Knight*, 1981; *Kelemen et al.*, 1997a]), parental liquid for the lower crust probably underwent crystal fractionation within the MTZ, and the MTZ gabbros are considered to represent the fractionated phases.

This 'igneous cumulate' origin of the MTZ gabbros also has also been demonstrated by their REE chemistry [*Kelemen et al.*, 1997a]. A positive Eu anomaly observed in the bulk rock REE pattern of the gabbro sills is consistent with the hypothesis that the gabbroic rocks represent fractionated crystalline phases and that residual liquid must have escaped from the system after the crystal fractionation, since mantle-derived melts at mid-ocean ridges have never been observed to have a positive Eu anomaly, whereas plagioclase in equilibrium with such melts has a large positive Eu anomaly. Similarly, the Mg numbers and the molar ratio of Ca/(Ca+Na) in the rocks are higher than in any mantle-derived melts. This, and the absence of zoning in the crystals, suggests that the rocks are the products of a one-stage crystal fractionation process, with subsequent removal of almost all remaining liquid. Because the oceanic crust attains its full thickness within a few kilometers of the axis at fast spread-

Table 5. Ion Microprobe Analyses of Clinopyroxenes

Sample	N^a	Ti	V	Cr	Sr	Y	Zr
95-41A	8	1700	260	4400	13	5	6
95-41B	9	1800	270	4500	12	5	7
95-42A	8	1700	250	3000	12	5	5
95-42B	11	1700	250	3900	13	5	5
95-P12	8	2100	330	3500	11	7	4
95-P13	8	1500	260	4500	13	5	4
96-44A	7	1900	290	3100	14	7	4
96-44B	6	1800	270	3100	14	6	8
96-44C	6	1600	250	3400	13	6	7
96-49A	7	1400	270	2800	24	5	3
96-49B	5	1700	290	2900	15	5	6
96-49C	6	1600	270	2000	14	5	5
96-54A	6	1700	270	3300	14	6	4
96-54B	6	1900	280	3600	12	6	6
96-67A	5	1900	300	4500	11	7	4
96-67B	7	1900	300	3900	12	7	4
96-67C	9	1900	300	4600	12	7	4
96-68A	8	1800	290	4000	11	6	4
96-68B	8	2000	290	4600	11	6	4
96-71	6	1800	270	4400	12	5	7
96-73	6	1700	260	4000	12	5	7
96-74	6	1800	260	4400	13	6	7
96-76A	6	1600	260	3500	12	4	6
96-76B	6	1700	260	4800	12	5	7

Values are in parts per million.
[a]Values denote number of analyses making up the average composition.

ing ridges [e.g., *Detrick et al.*, 1987], the crustal construction process must be confined to within a similar distance of the axis. Since the liquid extracted from the MTZ is likely to be parental to the overlying crustal rocks, geochemical data, along with seismic evidence for focused crustal accretion, suggest that the MTZ gabbros formed near the ridge axis.

On the basis of their field occurrence as sills, the formation of gabbroic rocks in the MTZ must have involved

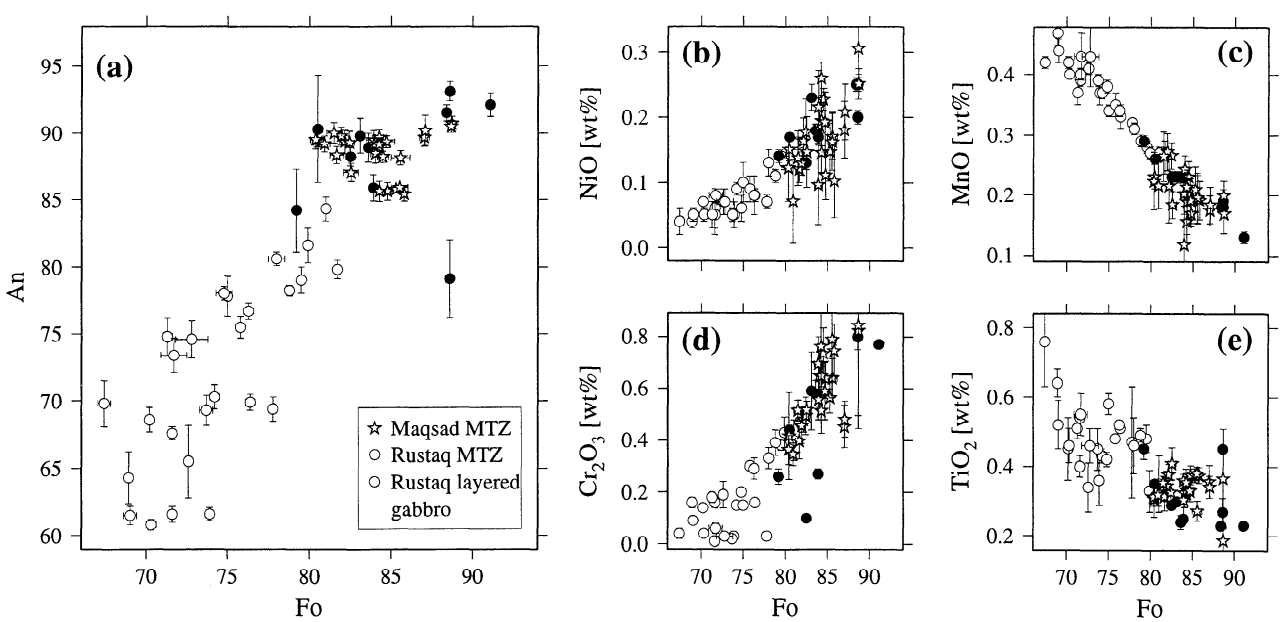

Figure 5. Geochemical covariations among Moho transition zone (MTZ) gabbros and lower crustal layered gabbros. Stars denote Maqsad MTZ gabbros analyzed. Solid and open circles denote MTZ gabbros and lower crustal gabbros in the Rustaq massif [*Browning*, 1982], respectively. One standard deviation is shown by error bars. (a) An content of plagioclase, (b) NiO and (c) MnO contents of olivine, and (d) Cr_2O_3 and (e) TiO_2 contents of clinopyroxene, plotted as a function of Fo content of coexisting olivine.

crystal fractionation processes in small, melt-filled lenses. The physicochemical processes in a melt lens depend on a number of factors including the cooling history and the form of open-system evolution. In a mid-ocean ridge environment, the cooling history of small-scale melt lenses at the Moho is dominantly controlled by the thermal evolution of the surrounding MTZ. Though the details of mid-ocean ridge thermal models depend on the assumed efficiency of hydrothermal heat removal, for a fast spreading ridge (half opening rate $\geq$50 mm/yr), the 1200°C isotherm crosses the base of the crust within ~7 km of the ridge axis in most models [e.g., *Lin and Parmentier*, 1989; *Chen and Morgan*, 1990; *Phipps Morgan and Chen*, 1993]. These thermal models are broadly consistent with the width of an axial low velocity zone observed at the East Pacific Rise [*Harding et al.*, 1989; *Vera et al.*, 1990; *Caress et al.*, 1992]. Melt lenses in the MTZ therefore would experience rapid cooling after being conveyed from the axis for ~0.15 m.y. at a half spreading rate of 50 mm/yr. The form of open-system evolution is also a function of distance from the ridge axis. Since melt migration in the mantle just beneath the crust must be highly focused toward the narrow (2-3 km) neovolcanic zone [e.g., *Macdonald*, 1982], fully open system evolution of MTZ melt lenses, characterized by frequent replenishment and expulsion, can be expected beneath the ridge axis. Seismic data suggest that the melt lenses should become closed after passing through the area beneath the neovolcanic zone.

Important constraints on possible processes in MTZ melt lenses include (1) the existence of modal layering, (2) compositional variations associated with the modal layering, and (3) no overall trend in mineral chemistry within the sills. The lack of an overall trend in mineral chemistry on the scale of a few meters, despite centimeter-scale compositional variations, is strong evidence that the gabbro sills resulted from open-system fractional crystallization; closed-system fractional crystallization would lead to progressive vertical trends within the sills. Though chemical diffusion through interstitial liquid or subsolidus reequilibration might obscure such a trend, it is impossible to preserve smaller-scale compositional variations that are observed while reequilibrating a chemical trend with a larger wavelength. The interpretation of the sills as relict, open-system melt lenses is also consistent with our interpretation of the geochemical relationship between the sills and the lower crustal gabbros; liquid extracted from MTZ melt lenses was parental to the overlying crustal rocks.

Modal layering can result from open-system behavior of melt lenses. Sudden replenishment by more primitive magma has two effects; it changes the melt composition in a melt lens toward a more primitive one [e.g., *O'Hara and Matthews*, 1981], and also it can promote a variety of fluid-dynamical phenomena, depending on the relative buoyancy of the replenishing magma [e.g., *Huppert and Sparks*, 1980; *Huppert et al.*, 1982; *Sparks and Huppert*, 1984]. Also, if expulsion is so drastic as to cause nearly complete drainage of the melt lens, any succeeding replenishment, whether continuous or sudden, will initiate a new cycle of fractionation. Therefore repeated drainage events with continuous magma input can result in modal layering. The normally and reversely graded layers could be explained as the products of crystallization at the top or bottom of melt lenses, respectively. Variations in compatible element composition and the relative absence of a systematic trend in incompatible components in the MTZ gabbro sills may be explained by a small degree of differentiation prior to melt extraction. The absence of a systematic variation in plagioclase composition is more difficult to explain; the fractionation of highly calcic plagioclase is discussed in section 5.2.

4.1. Possible Internal Causes for Modal Layering

The origin of modal layering has been a major focus in studies of mafic intrusions, and a number of different internal origins have been proposed, such as sedimentation from magmatic currents and double-diffusive convection, in addition to the external, open-system origin mentioned in the previous paragraph. As we demonstrate below, however, most of these internal mechanisms are unlikely to have formed layering in sills near the Moho in a mid-ocean ridge environment, which involves very slow cooling of small melt bodies. Whereas the thermal evolution of layered intrusions in continental crust is strongly related to the size of intrusions, the temperature of the small MTZ melt lenses is probably buffered by the ambient, hot MTZ. Even if the initial temperature of liquid at the MTZ is as hot as 1300°C, the melt lens would experience a temperature decrease of only about 100°C within the first 0.15 m.y, giving a lateral temperature gradient $\sim 10^{-2}$°C/m for a spreading rate of 100 mm/yr.

The effects of fractional crystallization from possible primary magmas are first considered here to provide a guideline for the following discussion. The differentiation of four candidate primary magmas (Table 6) was modeled using the method of *Grove et al.* [1992] with a modification by *Yang et al.* [1996]. Two of the candidates are the aggregate primary melts of *Kinzler and Grove* [1992] with different total degrees of mantle melting (14% for KG1, 18% for KG2). The others are two different estimates of the primary magma for the Oman ophiolite, based on the compilation of the crustal compositions, hereafter referred as OC1 for *Browning* [1982] and OC2 for *Pallister* [1984].

Except for OC2, which first fractionates plagioclase, the primary magmas follow the fractionation paths on which olivine, olivine + plagioclase, and olivine + plagioclase + clinopyroxene appear subsequently. This is in keeping with direct observations of the gabbros (interstitial clinopyroxenes) and experimental data at 200 MPa [e.g., *Baker and Eggler*, 1987; *Grove et al.*, 1992]. The estimated proportions of crystallizing phases on these multiply saturated paths are listed in Table 6. The important common features in all the calculated fractionation paths are that crystallization of plagioclase starts within a temperature range of 1225°C-1245°C (with the exception of OC1), and the liquid mass decreases by >1%/°C for the first 15 to 45% crystallization below the temperature of plagioclase saturation. In addition, the change in the liquid density is 1-3 kg/m^3 for the same increment.

Periodic deposition by crystal settling. Similarities of layered gabbros to sedimentary deposits led to the idea that modal layering originates in deposition from crystal-rich density currents, involving avalanches of crystals periodically detached from the roof and walls of a melt lens [*Wager and Brown*, 1968]. The periodic detachment of an

Table 6. Compositions of Primary Magmas Used in Modeling and Proportions of Crystallizing Phases

	Aggregate Primary Magma[a]		Oman Ophiolite Crustal Composition	
	KG1, $F = 14\%$	KG2, $F = 18\%$	OC1[b]	OC2[c]
SiO_2	49.0	47.8	52.0	51.1
TiO_2	0.88	0.81	0.62	0.60
Al_2O_3	16.8	17.0	13.5	16.6
FeO	7.85	8.29	7.14	7.20
MgO	11.6	12.4	13.5	9.2
CaO	11.9	12.1	10.9	12.8
K_2O	0.05	0.04	0.09	0.12
Na_2O	1.92	1.55	2.16	2.30
Mg#	72.5	72.7	77.1	69.5
Olivine%[d]	30	34	63	28
Plagioclase%[d]	70	66	37	72
Olivine%[e]	7	5	7	8
Plagioclase%[e]	40	42	50	43
Clinopyroxene%[e]	53	53	43	49

Values are in weight percent.

[a] Characteristics are polybaric, incremental batch, and accumulative melting of depleted mantle [*Kinzler and Grove*, 1992]. F is the total extent of melt achieved in melting column.

[b] Values are based on the compilation by *Browning* [1982].

[c] Values are based on the compilation by *Pallister* [1984]. The significant difference between OC1 and OC2, in spite of a similar compilation method, may be attributed to some fundamental difficulties inherent in the approach [*Thompson*, 1987].

[d] Values denote modal proportion on the olivine-plagioclase fractionation path.

[e] Values denote modal proportion on the olivine-plagioclase-clinopyroxene fractionation path.

upper thermal boundary layer is controlled by its convective instability [*Brandeis and Jaupart*, 1986]. If primary magma experiences $\leq 10\%$ crystal fractionation in total during its migration over a thickness of 500 m in the MTZ, with a crystallization rate of $\geq 1\%/°C$, the temperature gradient in the MTZ would be $\leq 1°C/50$ m, so an on-axis melt lens with a thickness of 5-50 m would have a temperature difference of $\leq 0.1°C$-$1°C$ within the melt lens. Therefore it seems unlikely that crystal nucleation and growth can be effectively confined within a thermal boundary layer, since the margins are cooler than the center by only a fraction of a degree.

Convection within a melt lens is another mechanism for crystal settling, and rhythmic sedimentation within a convecting melt lens has been suggested by *Sparks et al.* [1993], based on the concept of a critical concentration of crystals [*Koyaguchi et al.*, 1993]; the critical concentration is a function of crystal density, liquid density, and the temperature difference within the melt lens. This mechanism may have produced some of the observed layering in our samples. However, this is not certain. As pointed out by *Campbell* [1978], the rhythmic deposition of plagioclase (density of 2690-2700 kg/m^3 at 1200°C and 2 kbar for An_{85}-An_{90} [*Berman*, 1988]) might not be possible in some liquids derived by crystal fractionation of primary MORB (Figure 6b). Furthermore, gravitational sorting fails to explain reversely graded modal layering with a plagioclase-rich base [*Campbell*, 1978].

Kinetics of crystal nucleation and growth. Oscillatory nucleation is another suggested mechanism for layering in multicomponent magmatic systems [e.g., *Wager*, 1969; *Maaløe*, 1978; *Morse*, 1979]. If the crystallization of one phase near a eutectic point (or a cotectic line) can drive the melt composition into the stability field of another phase, this overshooting of the eutectic may occur repeatedly, resulting in oscillatory nucleation of the different phases. On the basis of the theoretical and numerical study by *Hort et al.* [1993], however, it can be shown that this type of overshooting is highly unlikely at the on-axis MTZ because of the very large cooling timescale of 0.05-0.15 m.y in this tectonic setting.

Double-diffusive convection. Since the experimental work by *Turner and Chen* [1974], the concept of double-diffusive layered convection has been investigated by petrologists [e.g., *McBirney and Noyes*, 1979; *Irvine*, 1980; *Sparks and Huppert*, 1984; *Browning*, 1984]. The required amount of thermal instability for double-diffusive convection is, however, too large to be attained by silicate magma [*McBirney*, 1985].

4.2. Possible Effects of Postcumulus Processes

So far, we have assumed that the small-scale compositional variations associated with modal layering are a primary igneous signature. If they were a "postcumulus" product, however, formation of sills in a closed system could not be confidently rejected because the resultant chemical trend in the sill as a whole could be modified by reaction between melt and ambient crystals before the postcumulus process of layer formation. An e-folding timescale (over which a chem-

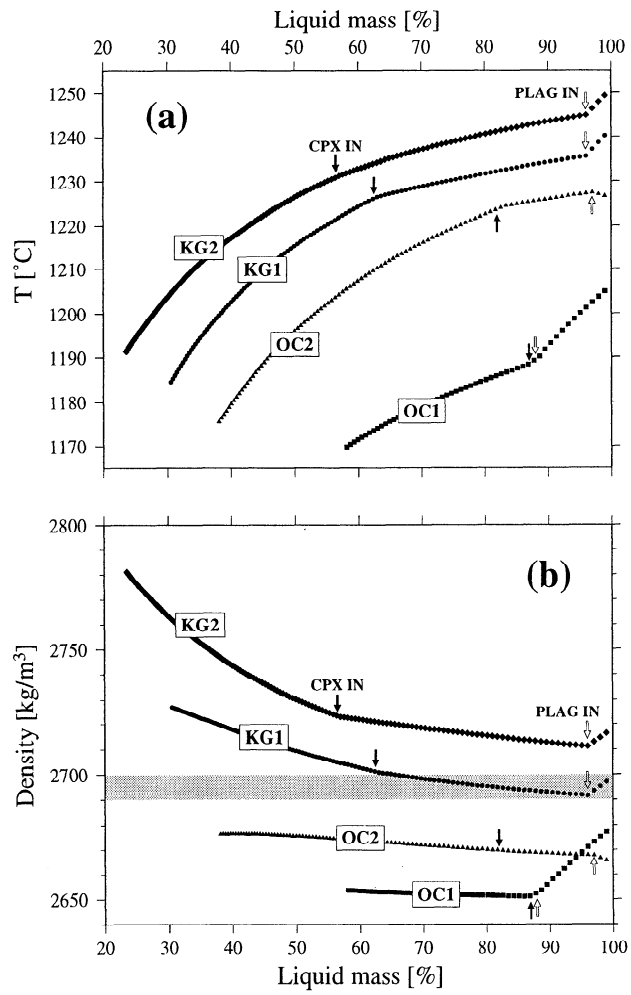

Figure 6. Results of fractional crystallization modeling. (a) Liquid temperature and (b) liquid density plotted as a function of liquid mass fraction remaining. Diamonds, circles, squares, and triangles denote the fractionation path starting from primary magma compositions of KG1, KG2 [*Kinzler and Grove*, 1992], OC1 [*Browning*, 1982], and OC2 [*Pallister*, 1984], respectively. These liquid compositions are given in Table 6. The system pressure was fixed at 200 MPa, and the liquid temperature was calculated using the liquid composition geothermometer of *Sisson and Grove* [1993] (Figure 6a). The liquid density was then calculated by the method of *Bottinga and Weill* [1970] with newer data on partial molar volume and thermal expansion coefficients [*Nelson and Carmichael*, 1979; *Bottinga et al.*, 1982; *Mo et al.*, 1982] (Figure 6b). Fe_2O_3 content is calculated using molar $Fe^{2+}/(Fe^{2+}+Fe^{3+}) = 0.9$. Open arrows show when plagioclase joins in fractionating olivine, except for OC2. OC2 first fractionates plagioclase then plagioclase + olivine. Solid arrows show when clinopyroxene joins the fractionating assemblage. Shaded zone in Figure 6b indicates the density range of plagioclase An_{85} -An_{90} at 1200°C and 2 kbar.

ical variation is decreased by $1/e$) due to liquid diffusion and melt/rock reaction in a porous system with a wavelength λ can be expressed as

$$\tau_e = \left(\frac{\lambda}{2\pi}\right)^2 \frac{1}{D_e}. \qquad (1)$$

where D_e is the effective diffusion rate defined as [*McKenzie*, 1984]

$$D_e = \left[\frac{(1-\phi)\rho_S}{\phi\rho_L}K_D + 1\right]^{-1} D_L, \qquad (2)$$

where ϕ, ρ_S, ρ_L, K_D, and D_L are cumulus porosity, matrix density, liquid density, crystal-liquid partition coefficient, and liquid diffusion rate, respectively. Local equilibrium between solid and liquid is assumed to be attained instantaneously, and this assumption can be tested by calculating a characteristic timescale for grain-scale diffusion,

$$\tau_g = \frac{a^2}{D_S}, \qquad (3)$$

where a and D_S are grain size and solid diffusion rate, respectively. The grain-scale diffusion time and the e-folding time are calculated for Fe-Mg interdiffusion in olivine and NaSi-CaAl interdiffusion in plagioclase (Figure 7). Since matrix porosity may vary spatially and temporally in a compacting crystal mush, the calculated e-folding time with a constant, relatively small porosity must be considered as a possible maximum; chemical diffusion would take place more rapidly for larger porosities (see (1) and (2)). Fe-Mg partitioning between olivine and adjacent liquid can quickly (<100 years) reach equilibrium, so the Fo variation across wavelengths as long as 10 m would be effectively erased within 0.1 m.y. NaSi-CaAl interdiffusion is, however, extremely slow, even under H_2O saturated conditions [*Liu and Yund*, 1992]. The absence of an overall trend in plagioclase composition within each sill therefore most likely is an original feature, formed during initial igneous crystallization of plagioclase.

The Fo compositional variation correlates well with the olivine modal proportion (Figure 4), and this type of covariation has been used as evidence for a postcumulus origin of compositional variation [e.g., *Chalokwu and Grant*, 1987; *Conrad and Naslund*, 1989]; the effect of reequilibration with trapped liquid, which lowers the Fo content, would be more prominent at a smaller olivine proportion. However, this mechanism fails to explain the correlation of Fo content in olivine with Cr content in clinopyroxenes, because the modal proportion of clinopyroxene does not change sympathetically with that of olivine. Cr diffusion in clinopyroxene is probably slow, owing to its trivalent nature [*Hofmann*, 1980; *Sneeringer et al.*, 1984], suggesting that Cr variation reflects conditions of primary crystallization. The correlations among modal layering, Fo, and Cr contents are thus better explained as a preserved primary signature, not a secondary postcumulus product.

If the centimeter-scale Fo variation is a primary igneous feature, as suggested above, Figure 7b indicates an intriguing constraint on the process of cumulate formation. Since chemical diffusion through the interconnected liquid phase can rapidly damp out centimeter-scale variation, cumulus porosity must have been very small to effectively isolate remaining melt pockets. It would be very difficult to obtain such a low porosity by crystal settling, and porosity reduction by postcumulus compaction has a much longer timescale ($>10^3$ years, *Sparks et al.*, [1985, Figure 8]) than the diffusive damping timescale. Since crystal nucleation requires a finite amount of undercooling, it is likely that heterogeneous nucleation and growth within a thermal boundary layer are dominant processes within a slowly cooling melt lens because of the

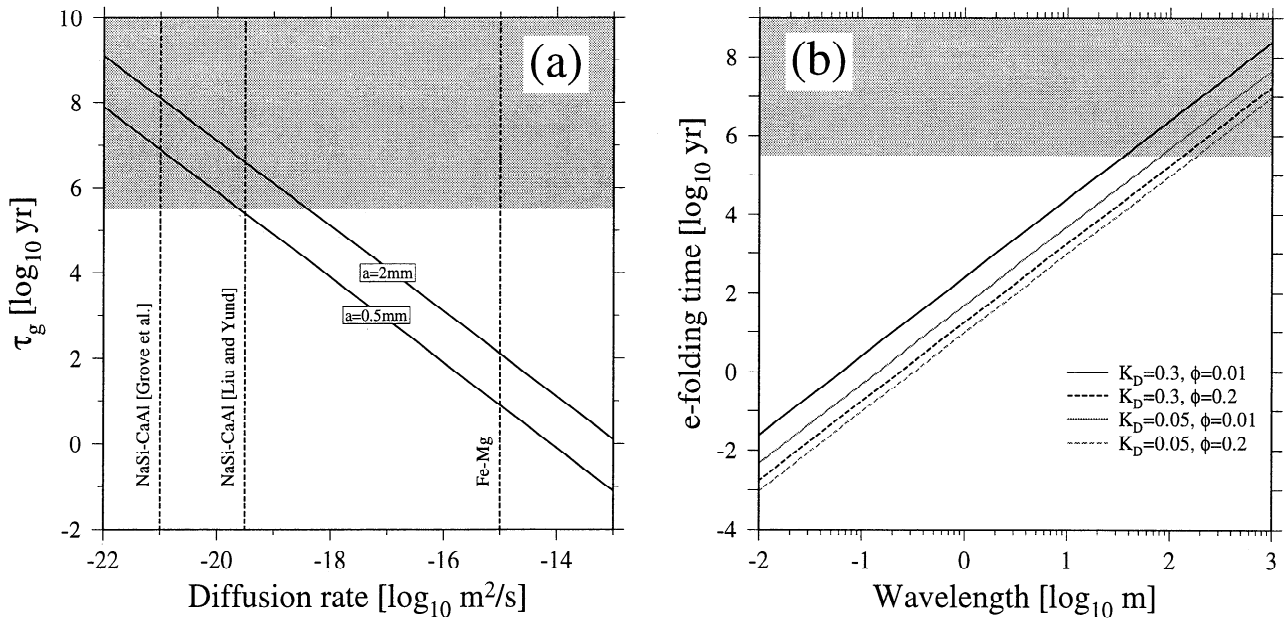

Figure 7. (a) Grain-scale diffusion time for two grain sizes (0.5 and 2 mm) as a function of solid diffusion rate. Representative diffusion rate for olivine and plagioclase compositions are shown by dashed lines: Fe-Mg interdiffusion in olivine at 1200°C [*Buening and Buseck*, 1973], NaSi-CaAl interdiffusion in plagioclase at 1200°C [*Grove et al.*, 1984], and at 1050°C saturated with H_2O [*Liu and Yund*, 1992]. (b) The *e*-folding time as a function of chemical variation wavelength. Liquid diffusion rate D_L is assumed to be 10^{-10} m^2/s [e.g., *Brady*, 1995]. Solid lines show the case of 1% porosity, while dashed lines show 20% porosity. Two different partition coefficients (K_D=0.05 and 0.3) are used to encompass possible variations in NaSi-CaAl and Fe-Mg partition coefficients. Chemical diffusion in the MTZ would be effectively blocked after 0.15 m.y. because of cooling, and the time larger than the critical time is shaded.

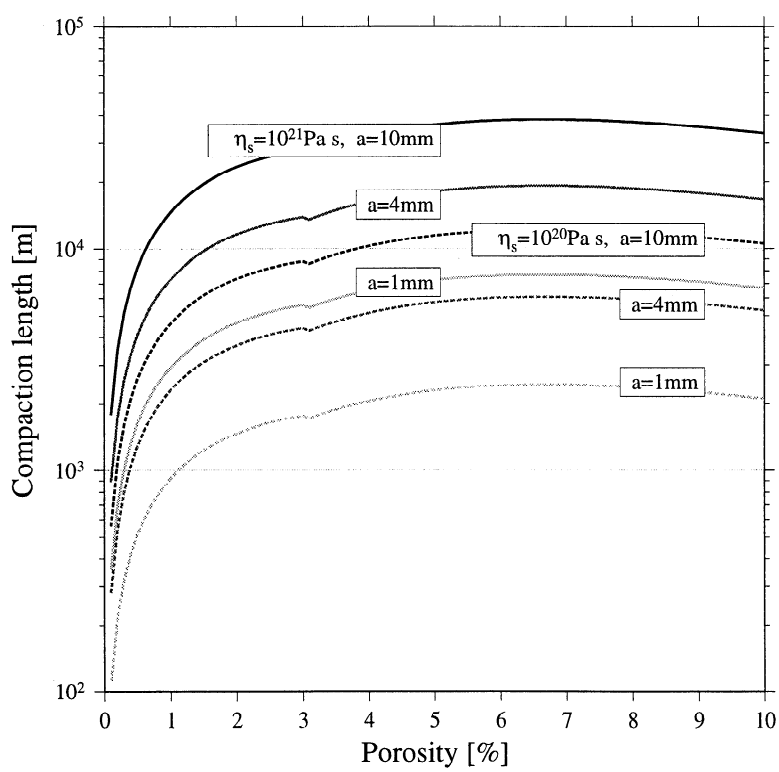

Figure 8. Compaction length plotted as a function of porosity. Dependencies of permeability on porosity and grain size follow those of *McKenzie* [1989]. Matrix viscosity is also a function of porosity, and we adopt the relation $\eta(\phi) = \eta(0)\exp(-45\phi)$, derived by *Kelemen et al.* [1997b] from the experimental data of *Hirth and Kohlstedt* [1995a, 1995b]. Solid lines denote the compaction length using the melt-free matrix viscosity $\eta(0)$ of 10^{21} Pa s, while dashed lines show the case of 10^{20} Pa s. A value of 10 Pa s is used for melt viscosity.

smaller interfacial energies involved [e.g., *Kirkpatrick*, 1977; *Dowty*, 1980]. Thus in situ cumulate formation is the most likely explanation for the preserved, centimeter-scale Fo variation. Minerals probably nucleated and grew directly on the contacts of small, melt-filled lenses, and then liquid was removed by Poiseuille flow from the open melt lens rather than by compaction of a crystal mush.

Crystal aging models for modal layering are founded on possible positive feedbacks in postcumulus crystallization processes, activated either by chemical diffusion through porous fluid [*Boudreau*, 1994, 1995] or by the flow of porous fluid itself [A. E. Boudreau and A. R. McBirney, submitted to Journal of Petrology, 1996]. These mechanisms may be applicable to formation of millimeter-scale modal layering in our samples, which is not correlated with cryptic variation. For centimeter-scale modal layering in our samples, which is correlated with chemical variation, these mechanisms cannot have been important; the liquid diffusion or advection required to make modal layering would have erased the compositional variations.

5. Discussion

5.1. Possible Mechanisms of Sill Formation

It may be counterintuitive to expect magmatic sills in an extensional tectonic environment such as beneath mid-ocean ridges, because the greatest extensional stress is horizontal, preferring dike formation. Accumulation of dike intrusions may gradually compensate for extensional horizontal strain, leading to a stress condition that prefers sill formation [*Gudmundsson*, 1990; *Rubin*, 1990]. The stress state at the Moho level is, however, probably decoupled from that at the upper crustal dike sequences, for example, owing to the existence of a midcrustal melt lens.

Apart from this idea, two different models for sill formation near the Moho have been proposed on the basis of the dynamics of focused mantle flow. *Rabinowicz et al.* [1987] suggested that a region with an excess porosity in the upwelling mantle (e.g., a magma "soliton") would result in formation of a melt lens in the region of mantle overturn, just beneath the Moho. The typical wavelength of magmatic solitons is comparable to the compaction length, which is defined as [*McKenzie*, 1984]

$$\delta_c = \sqrt{\frac{k_\phi \left(\xi + \frac{4}{3}\eta\right)}{\mu}}. \tag{4}$$

ξ and η are bulk and shear viscosities of the matrix, respectively, and k_ϕ is permeability, which is a function of porosity and grain size. Beneath a normal mid-ocean ridge, the melt-free solid viscosity is estimated to be between 10^{20} and 10^{21} Pa s at depths $\leq$35 km [*Hirth and Kohlstedt*, 1996], so compaction length is of the order of 10^3-10^4 m (Figure 8). Therefore, very few sills would be formed within the MTZ by this mechanism. Gabbro sills in the MTZ are much more numerous than this.

In another hypothesis, *Ildefonse et al.* [1993] noted that stress field rotation may be associated with focused mantle flow beneath a spreading center and suggested that the resultant vertical extensional stress field is responsible for sill formation. The rotation of the stress field, however, occurs far from the ridge axis (>10 km) in the numerical model [*Rabinowicz et al.*, 1987, Figure 5] on which the Ildefonse et al. hypothesis is based. Melt lenses >10 km off axis probably cannot contribute to the crustal construction beneath the neovolcanic zone. We also note that the plausibility of focused mantle flow itself has been the subject of debate [e.g., *Forsyth*, 1992; *Spiegelman*, 1993; *Hirth and Kohlstedt*, 1996], particularly for fast spreading ridges [e.g., *Lin and Phipps Morgan*, 1992].

Kelemen et al. [1997a] proposed that the MTZ sills may represent liquid ponds due to permeability barriers, which are created by crystallization during porous flow. Melt migration in the upper mantle beneath mid-ocean ridges may be dominated by focused porous flow [e.g., *Kelemen et al.*, 1995a, 1995b; *Aharonov et al.*, 1995] or by hydrofracture [e.g., *Maaløe*, 1981; *Nicolas*, 1986, 1990]. Ophiolite mantle sections have geological features formed by both types of melt transport, i.e., replacive dunites formed by porous flow and pyroxenite and gabbro dikes formed by hydrofracture. *Kelemen et al.* [1997b] concluded, however, that hydrofracturing is generally unlikely in the adiabatically upwelling mantle beneath a ridge axis and must primarily be formed near the Moho and in conductively cooled mantle lithosphere, based on the geochemistry of the mantle dikes and the rheology of partially molten peridotite.

In any case, the Oman MTZ contains abundant evidence for porous flow of magma, locally with very high porosities [e.g., *Ceuleneer and Rabinowicz*, 1992; *Nicolas and Boudier*, 1995; *Boudier and Nicolas*, 1995]. Even if magma transport in fractures below the MTZ is an important melt migration mechanism, the presence of anelastic, melt-rich regions at the MTZ would generally impede fracture propagation. Instead, melt would be trapped in sills. In this paper and a companion paper [*Kelemen and Aharonov*, 1997], we concentrate on melt extraction from gabbros at and above the MTZ.

The thermal impact of porous melt flow on the surrounding mantle can be estimated by calculating the thermal Peclet number, defined as

$$Pe = \frac{wr}{\kappa}, \tag{5}$$

where w is flow rate and r is pore width. Assuming that melt migration in the MTZ is mainly confined to an area directly beneath the neovolcanic zone, the porous flow rate can be estimated as

$$w = \frac{H_C V}{W_V \chi \phi}, \tag{6}$$

where H_C, V, W_V, and χ are crustal thickness, full spreading rate, width of the neovolcanic zone, and the volume proportion of melt transport conduits within mantle peridotite, respectively. The pore width is calculated using the relation $r \sim 0.13 a \phi^{1/2}$ [*Hart*, 1993], where a is grain size. Thus the Peclet number can be expressed as follows:

$$Pe = \frac{0.13 a H_C V}{\kappa \chi \phi^{\frac{1}{2}} W_V}. \tag{7}$$

Substituting a = 1-10 mm, ϕ = 0.01-0.10, $\kappa = 10^{-6}$ m^2/s, H_C = 6 km, V = 100 mm/yr, and W_V = 2 km and assuming χ = 1 (diffuse porous flow throughout the MTZ), the Peclet

number ranges from 4×10^{-6} to 1×10^{-4}, which indicates that the melt temperature is the same as the temperature of the surrounding mantle. Therefore the presence of gabbro sills is direct evidence that the paleotemperature at the MTZ was ~1225°C-1250°C where mantle-derived basalts become saturated in plagioclase. As the melt crosses the saturation surfaces for plagioclase and clinopyroxene and migrates following the ambient geothermal gradient, it starts to fractionate a substantial proportion of crystals, >1%/°C for the next 15 to 45% crystallization (Figure 6a). The geothermal gradient would not be disturbed significantly by latent heat release due to crystallization because of slow crystallization and low melt/rock ratio. Porosity would tend to decrease owing to crystallization. At the same time, the increased fluid pressure gradient due to decreasing porosity would lead to matrix deformation, which would tend to maintain the initial porosity. The matrix deformation timescale can be expressed as [*McKenzie*, 1984]

$$\tau_v = \frac{\delta_c}{w}, \tag{8}$$

and the crystallization timescale may be written as

$$\tau_c = \left(w \frac{dT}{dz} \frac{df}{dT} \right)^{-1}, \tag{9}$$

where dT/dz is the geothermal gradient and df/dT is the degree of fractionation due to temperature decrease. Near the Moho, at temperatures less than 1300°C, the mantle viscosity is probably $\sim10^{21}$ Pa s [*Hirth and Kohlstedt*, 1996]. Thus, with melt viscosity ~10 Pa s, porosity $\geq$1.5%, and grain size $\geq$ 4 mm, the compaction length is likely to be $\geq10^4$ m (Figure 8). For probable ranges of dT/dz (0.01-0.02 °C/m) and df/dT (0.01-0.03 °C^{-1}; see Figure 6), $\tau_v \geq \tau_c$, and so the matrix probably cannot deform fast enough to keep the pore space open.

This mechanism of crystallization in pore space probably accounts for the abundance of peridotites impregnated with plagioclase [*Ceuleneer and Rabinowicz*, 1992; *Boudier and Nicolas*, 1995], as well as for gabbro sills in the Oman MTZ. Therefore the formation of permeability barriers may be a corollary to low Peclet number porous melt flow entering a conductively cooling regime, where plagioclase begins to crystallize. While the gabbro sills in the MTZ are observed near the center of a presumed mantle diapir [e.g., *Nicolas and Boudier*, 1995], mafic cumulates in dikes and sills located far below the Moho in the harzburgite mantle section are distributed concentrically to the diapir [*Ceuleneer et al.*, 1996]. The relationship between the distribution of these melt relics and the possible diapiric thermal structure is consistent with the impermeable barrier hypothesis described above.

Accumulation of incoming melts beneath an impermeable barrier increases pore fluid pressure, and this overpressure may result in sill formation either by brittle failure or ductile deformation of MTZ dunites. If overpressurization due to ductile deformation exceeds the tensile strength of the surrounding dunites but not the overlying barrier, sills would be formed as lateral fractures. *Kelemen et al.* [1997b] provided a minimum estimate of the tensile strength of partially molten dunite as 50 MPa. The amount of excess pressure resulting from ductile deformation can be estimated using the governing equations for viscously deformable porous media [*McKenzie*, 1984]. For a simplified case of one-dimensional flow with constant porosity, the fluid pressure gradient may be written as

$$\frac{\partial p}{\partial z} = \frac{\mu}{k_\phi}\phi(w - W) \sim \frac{\mu}{k_\phi}\phi w \tag{10}$$

where p and W are excess fluid pressure (relative to lithostatic pressure) and matrix velocity, respectively. The matrix deformation is significant within one compaction length, so that the associated overpressure can be estimated as

$$\Delta p \sim \frac{\partial p}{\partial z}\delta_c \sim \frac{\mu}{k_\phi}\phi w \delta_c. \tag{11}$$

Figure 9 shows the calculated overpressure as a function of porosity, with effects of changing matrix viscosity and grain size. The rheology of the mantle peridotites is very sensitive to porosity and grain size, so that possible regional variations in these two parameters could account for both brittle and ductile formation of MTZ sills. The two contrasting types of contacts between gabbros and dunites, i.e., sharp and diffuse contacts, may reflect this sensitivity.

Most likely, further melt accumulation will eventually break the overlying permeability barrier, followed by crack propagation driven by overpressure and melt buoyancy. A quantitative model for this process is presented by *Kelemen and Aharonov* [1997]. Though the sill overpressure decreases as liquid escapes, one expulsion event may effectively dry up the sill because of melt buoyancy. Also, as shown by *Kelemen and Aharonov* [1997], pressure changes due to fracture formation can change the proportion of crystallizing phases, producing modal layering.

Sills formed beneath a permeability barrier and periodically emptied by hydrofracture would follow open-system chemical evolution characterized by slow, continuous replenishment and rapid, episodic expulsion. The lack of overall trends in the mineral chemistry of the gabbro sills is easily explained in this fashion, and the modal layering and compositional variations can be explained by frequent drainage events and in situ crystallization at the margins of slowly cooling melt lenses. To preserve the correlated centimeter-scale compositional variation [e.g., *Korenaga and Kelemen*, 1997], sills replenished by porous flow from below must have accreted from the top down, with each new melt lens forming beneath the permeability barrier created by crystallization in and immediately around the previous melt lens. In addition, though density currents, crystallization kinetics, and double-diffusive convection can be reasonably rejected as the origin of the modal layering, rhythmic sedimentation in a thermally or compositionally convecting melt lens may remain plausible for normally graded layers, especially those which are not accompanied by clear compositional variations.

5.2. Size of MTZ Melt Lens and Proportion of Crystal Fractionation

Using a simple Rayleigh fractionation model, the height of the original melt lens H can be estimated from compositional variation data as [e.g., *Browning*, 1984]

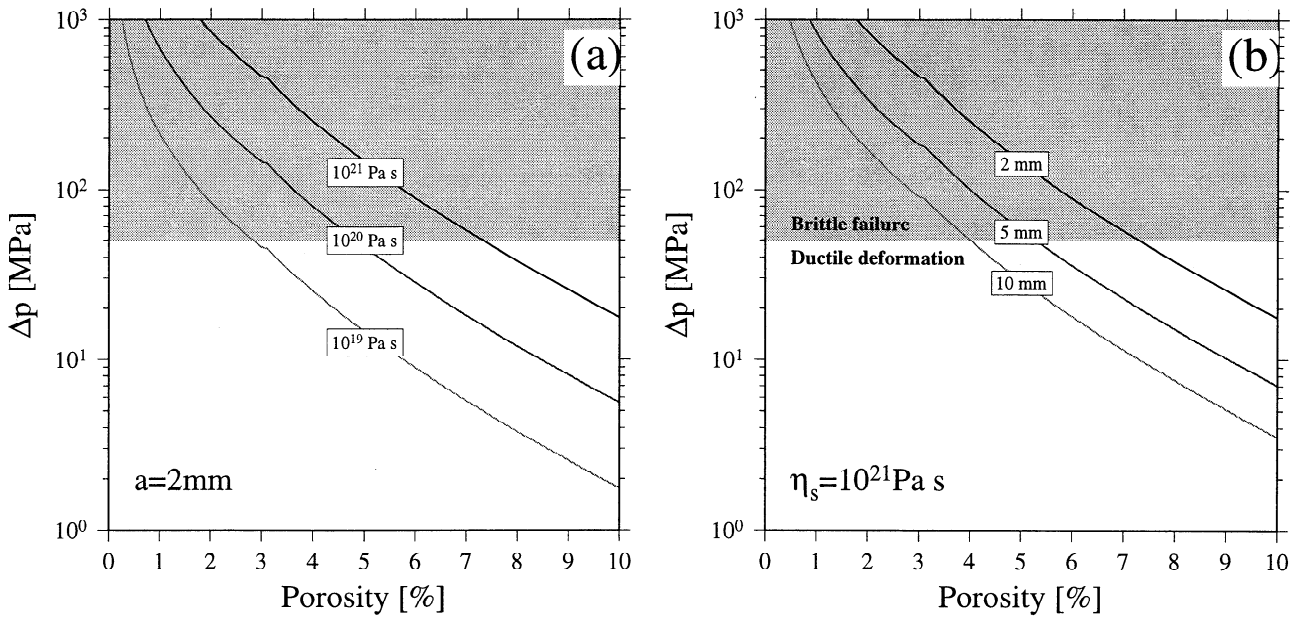

Figure 9. Overpressure in the melt phase caused by viscous deformation of the porous matrix, calculated as a function of porosity. (a) Effect of changing melt-free matrix viscosity $\eta(0)$. Matrix grain size is fixed at 2 mm. (b) Effect of changing matrix grain size. Here 10^{21} Pa s is used for melt-free matrix viscosity, and $w\phi$ is assumed to be 9.5×10^{-9} m/s (equation (6)). Overpressure larger than 50 MPa is shaded where brittle failure would occur instead of ductile deformation.

$$H = h\left[1-\left(\frac{C^f}{C^i}\right)^{\frac{1}{D_b-1}}\right]^{-1}, \qquad (12)$$

where h, C^i, C^f, and D_b are cumulate layer height, initial and final concentrations of a particular element in crystal, and bulk distribution coefficient, respectively. We use the Cr_2O_3 contents of clinopyroxene for this calculation, assuming negligible influence of the fractionation of Cr-rich minerals such as Cr-spinel. Using $D_{Cr}^{Ol/liq} = 2$, $D_{Cr}^{Cpx/liq} = 10$, and $D_{Cr}^{Pl/liq} = 0.01$ [*Cox et al.*, 1979], the bulk distribution coefficient would be ~4 with the typical mass proportions of 25% olivine, 35% clinopyroxene, and 40% plagioclase. Data for sample 96-76, for example, suggest that h = 60 mm, C^f = 0.5 wt%, and C^i = 0.7-1.0 wt% (Figure 4), so that the melt lens height would be ~30-60 cm. More subtle variations yield larger estimates of lens height, such as ~120 cm for sample 96-71. These results are similar to those of *Browning et al.* [1989] for cumulate gabbros in the Troodos ophiolite. Note that the gabbro sills in the MTZ may have undergone flattening during deformation subsequent to the formation of the layering, so these height estimates probably represent minima. However, the ratio of layer thickness to original melt lens is more robust and may be used to estimate the mass proportion of initial liquid represented by a gabbro layer. In the case of the gabbro sills in the Oman MTZ, the degree of crystallization in MTZ melt lenses is thus 5-20%, at most (considering the influence of Cr-rich minor phases), consistent with the very small variations in the TiO_2 content observed in these rocks.

The lack of a systematic trend in the plagioclase composition remains enigmatic. We suggest that when liquid has high normative anorthite/albite, the change in the plagioclase composition due to crystal fractionation may be much smaller than the accompanying change in the olivine composition and therefore that it is hard to detect the resulting trend in the plagioclase composition. Figure 10 shows the relation between coexisting olivine and plagioclase compositions according to the fractional crystallization modeling described above. For the most calcic initial liquid composition (KG2), the change in the plagioclase composition is less pronounced than the change in the olivine composition.

We note that none of the proposed primary melts used in modeling is able to reproduce the observed plagioclase composition ($An_{85.4}$ - $An_{90.7}$). The Oman ophiolite gabbros are, in general, more calcic than other oceanic gabbros [e.g., *Meyer et al.*, 1989], except for those from the crust/mantle transition zone at the East Pacific Rise [*Dick and Natland*, 1996]. Though a high degree of melting and/or significant H_2O in the melts may account for the observed calcic nature of plagioclase [*Pallister and Hopson*, 1981], it is still difficult to incorporate the effect of H_2O in a quantitative model of fractional crystallization [*Panjasawatwong et al.*, 1995]. Figure 10 suggests, however, that the rate of change of plagioclase composition will become much smaller than the rate of change of olivine composition when the crystallizing plagioclase has very high An contents.

Although a few lines of geophysical evidence have been reported for the presence of a low-velocity zone around the axial Moho [e.g., *Garmany*, 1989; *Dunn et al.*, 1994], so far, MTZ melt lenses have not been successfully imaged by seismic reflection experiments. Highly attenuative axial lower crust [*Wilcock et al.*, 1992] may significantly damp possible reflections from MTZ melt lenses, and the dimensions of MTZ gabbro sills may not necessarily represent the actual sizes of MTZ melt lenses. As suggested by the

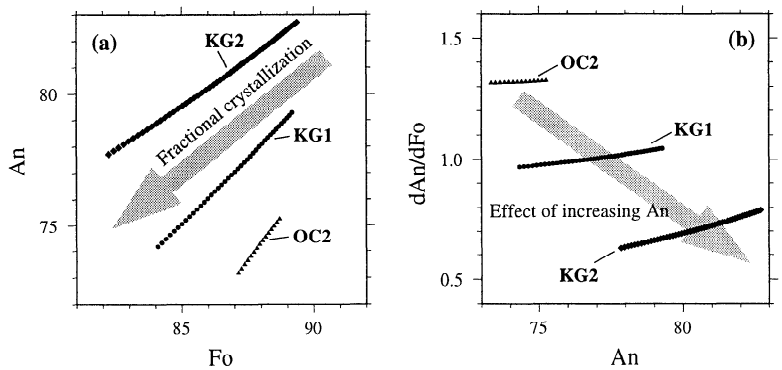

Figure 10. (a) Olivine-plagioclase compositional trend according to fractional crystallization modeling (Figure 6 and Table 6). Diamonds, circles, and triangles denote the fractionation paths starting from primary magma compositions KG1, KG2, and OC2, respectively. (b) Change in the plagioclase composition divided by the change in the coexisting olivine (dAn/dFn) plotted as a function of the An content.

Cr_2O_3 variations, melt lenses may be very thin (e.g.,~1 m), far below the vertical resolution of reflection experiments. Crystals can continue to accumulate in growing sills through the cycles of melt replenishment and expulsion. The low-velocity zone around the Moho may be better interpreted as an integrated effect of several thin magmatic layers.

5.3. Genesis of the Oceanic Lower Crust

Whereas the lower crustal layered gabbros show progressive chemical differentiation (Figure 5), there is no obvious, overall trend in the stratigraphic variations of their mineral chemistry [*Pallister and Hopson*, 1981; *Smewing*, 1981; *Browning*, 1982; *Ernewein et al.*, 1988]. Though these observations were originally used to infer the open-system evolution of a large-scale magma chamber, they were later proposed to be consistent with crustal generation entailing a small-scale, midcrustal, axial melt lens [e.g., *Phipps Morgan and Chen*, 1993; *Quick and Denlinger*, 1993; *Henstock et al.*, 1993]. In this view, the lower crust is constructed by ductile flow downward from the open-system axial melt lens. Such ductile flow models, however, predict exceptionally large strains in the lower crust, and it seems unlikely that such ductile flow can preserve the modally graded layers observed in the lower crustal gabbros.

Other doubts about this model relate to the physics of ductile flow. Intercrystalline glide lubricated with a large fraction of melt (>20%) [*Van der Molen and Paterson*, 1979; *Wickham*, 1987; *Nicolas et al.*, 1993] was thought to be required to explain the absence of extensive intracrystalline plastic deformation in the layered gabbros [e.g., *Benn and Allard*, 1989; *Nicolas*, 1988; *Quick and Denlinger*, 1993]. Seismic constraints on the possible melt fraction in the lower crust probably preclude such a large melt fraction [e.g., *Caress et al.*, 1992; *Phipps Morgan et al.*, 1994]. A hybrid deformation model proposed by *Nicolas et al.* [1996] suggests that this difficulty might be overcome if intercrystalline glide is coupled with local diffusion creep where grain boundaries impinge at high angles. Also, recent modeling of seismic properties of partially molten rocks with anisotropic melt distributions suggests that porosities as high as 35-50% could be present in the axial lower crust [D. Mainprice, submitted to Tectonophysics, 1996]. However, regardless of the amount of melt, the requirement for an interconnected melt phase for lubricated crystalline glide appears to conflict with the mineral chemistry evidence emphasized in this paper; since the level of neutral buoyancy is located at a depth of less than 2 km below the seafloor [*Hooft and Detrick*, 1993], melt in lower crustal gabbros with high, interconnected porosities would migrate upward through the porous network, destroying the observed correlations between mineral compositions in the layered gabbros [*Korenaga and Kelemen*, 1997] .

The discussion of low Peclet number porous melt flow in a conductively cooling solid matrix suggests that permeability barriers would eventually build up by crystallization in the pore space. Though the rheology of lower crustal gabbro is poorly known, this may occur within the lower crust as well as in the MTZ. Striking similarities between layered gabbros and MTZ gabbro sills led *Kelemen et al.* [1997a] to suggest that the oceanic lower crust may be constructed as "sheeted sills", i.e., intrusion of multiple sills at a variety of depths, in a model conceptually similar to that of *Bedard et al.* [1988]. Permeability barriers created by diffuse porous flow would provide a physically plausible mechanism for the formation of magmatic sills in the axial lower crust. Multiple sill formation at a variety of depths can produce the observed lack of regular chemical trends in the lower gabbros as a whole. Except for the work of *Browning* [1982] on a modally graded layer from Wadi Shafan in the Rustaq massif, fine-scale chemical analysis of modal layering has not yet been applied to the layered gabbros in Oman. Such analysis could help to decipher the origin of the modal layering in the lower crust.

The permeability barrier mechanism also seems to be applicable to the formation of the midcrustal melt lens. The depth of the melt lens does not correspond to the level of neutral buoyancy, and it is probably better understood as the possible upper limit of gabbroic crystallization, imposed by vigorous hydrothermal cooling [*Phipps Morgan and Chen*, 1993; *Chen and Phipps Morgan*, 1996]. In other words, the midcrustal melt lens may represent a liquid pond beneath the uppermost permeability barrier, above which the thermal gradient is so steep that porous melt flow would be rapidly frozen.

6. Summary

On the basis of the following geochemical and geophysical arguments, we conclude that the most likely explanation for gabbro sills in the Oman ophiolite MTZ is in situ fractional crystallization along the edges of a small-scale, open-system melt lens, characterized by continuous replenishment and episodic expulsion beneath the ridge axis:

1. Correlations in mineral chemistry in gabbros in the MTZ and in the lower crust imply that the liquid from which the MTZ gabbros crystallized was parental to the crustal rocks.

2. The lack of an overall, vertical trend in mineral chemistry within individual gabbro sills is strong evidence that MTZ melt lenses evolved as open systems. Very slow diffusion rates for plagioclase components support the hypothesis that this lack of trend is a primary signature, not a product of postcumulus processes.

3. Completion of crustal construction at fast spreading ridges in less than 0.05 m.y. limits possible open-system behavior of melt bodies off axis. Therefore open-system fractional crystallization within the MTZ melt lenses must have been largely restricted to an area directly beneath the ridge axis.

4. Since the temperature of MTZ melt lenses tends to be buffered by the large-scale mid-ocean ridge thermal evolution, the cooling rate of the melt lenses near the ridge axis is slower than 1°C/1000 years, and the temperature difference within the melt lenses is smaller than 1°C.

5. It is unlikely that the modal layering observed in the MTZ gabbros had an "internal" cause, such as gravitational currents, oscillatory nucleation, or double-diffusive convection, because of the slow cooling rate and the small temperature difference in melt lenses.

6. Crystal settling would result in relatively high porosities, which could not preserve the observed small-scale compositional variations. In situ crystallization directly on the edges of melt lenses would be favored by the thermal environment.

7. The correlated compositional variations in the Oman lower gabbros preclude the possibility that the main mechanism of melt transport from the Moho to the base of the sheeted dikes is diffuse porous flow. Instead, the dominant mechanism of melt transport must have been focused flow, such as flow in cracks.

8. Melt migration by low Peclet number porous flow, entering a conductively cooling regime, probably stagnates beneath permeability barriers, where plagioclase begins to crystallize. Resultant liquid ponds would repeatedly undergo episodic hydrofracture [*Kelemen and Aharonov*, 1997]. One expulsion could reset the melt lens composition by nearly complete drainage, so that repetitious expulsion would result in modal layering.

Acknowledgments. We thank Hilal Al Azri, Françoise Boudier, Benoit Ildefonse, Adolphe Nicolas, Greg Hirth, Ken Koga, Rachel Cox, and Emilie Hooft for generous assistance in the field. This paper has benefited from constructive discussions with Greg Hirth, Graham Kent, Ken Koga, Takehiro Koyaguchi, Dan Lizarralde, Peter Meyer, Nobu Shimizu, and Jack Whitehead. J.K. especially thanks Ken Koga for his guidance in geology and geochemistry throughout this work and for providing digitized field maps used in Figure 1. We also thank Nil Chatterjee for assistance with the MIT electron microprobe, Nobu Shimizu and Graham Layne for assistance with the Woods Hole ion microprobe, and Henry Dick for assistance with petrographic analysis. Bob Detrick, Greg Hirth, Steve Holbrook, Marcia McNutt, Alexander McBirney, John Sinton, Alan Boudreau, and Bill Meurer reviewed the manuscript and provided helpful comments. This work was supported by NSF grants OCE-9416616 and OCE-9416631. Woods Hole Oceanographic Institution contribution 9590.

References

Aharonov, E., J. A. Whitehead, P. B. Kelemen, and M. Spiegelman, Channeling instability of upwelling melt in the mantle, *J. Geophys. Res.*, *100*, 20,433–20,450, 1995.

Alabaster, T., J. A. Pearce, and J. Malpas, The volcanic stratigraphy and petrogenesis of the Oman ophiolite complex, *Contrib. Mineral. Petrol.*, *81*, 168–183, 1982.

Albee, L. A., and L. Ray, Correction factors for electron probe microanalysis of silicates, oxides, carbonates, phosphates, and sulfates, *Anal. Chem.*, *42*, 1408–1414, 1970.

Baker, D. R., and D. H. Eggler, Composition of anhydrous and hydrous melts coexisting with plagioclase, augite, and olivine or low-Ca pyroxene from 1 atm to 8 kbar: Application to Alcutian volcanic center of Atka, *Am. Mineral.*, *72*, 12–28, 1987.

Bedard, J. H., R. S. J. Sparks, R. Renner, M. J. Cheadle, and M. A. Hallworth, Peridotite sills and metasomatic gabbros in the Eastern Layered Series of the Rhum Complex, *J. Geol. Soc. London*, *145*, 207–224, 1988.

Bence, A. E., and A. L. Albee, Empirical correction factors for the electron microanalysis of silicates and oxides, *J. Geol.*, *76*, 382–403, 1968.

Benn, K., and B. Allard, Preferred mineral orientations related to magmatic flow in ophiolite layered gabbros, *J. Petrol.*, *30*, 925–946, 1989.

Benn, K., A. Nicolas, and I. Reuber, Mantle-crust transition zone and origin of wehrlitic magmas: Evidence from the Oman ophiolite, *Tectonophysics*, *151*, 75–85, 1988.

Berman, R. G., Internally-consistent thermodynamic data for minerals in the system Na_2O-K_2O-CaO-MgO-FeO-Fe_2O_3-Al_2O_3-SiO_2-TiO_2-H_2O-CO_2, *J. Petrol.*, *29*, 455–522, 1988.

Bottinga, Y., and D. F. Weill, Densities of liquid silicate systems calculated from partial molar volumes of oxide components, *Am. J. Sci.*, *269*, 169–182, 1970.

Bottinga, Y., D. F. Weill, and P. Richet, Density calculations for silicate liquids, I, Revised method for aluminosilicate compositions, *Geochim. Cosmochim. Acta*, *46*, 909–920, 1982.

Boudier, F., and A. Nicolas, Nature of the Moho Transition Zone in the Oman ophiolite, *J. Petrol.*, *36*, 777–796, 1995.

Boudier, F., J. L. Bouchez, A. Nicolas, M. Cannat, G. Ceuleneer, M. Misseri, and A. Montigny, Kinematics of oceanic thrusting in the Oman ophiolite: Model of plate convergence, *Earth Planet. Sci. Lett.*, *75*, 215–222, 1985.

Boudier, F., A. Nicolas, and B. Ildefonse, Magma chambers in the Oman ophiolite: Fed from the top or the bottom?, *Earth Planet. Sci. Lett.*, *144*, 239–250, 1996.

Boudreau, A. E., Mineral segregation during crystal aging in two-crystal, two-component systems, *S. Afr. J. Geol.*, *97*, 473–485, 1994.

Boudreau, A. E., Crystal aging and the formation of fine-scale igneous layering, *Mineral. Petrol.*, *54*, 55–69, 1995.

Brady, J. B., Diffusion data for silicate minerals, glasses, and liquids, in *Mineral Physics and Crystallography: A Handbook of Physical Constants, AGU Ref. Shelf*, vol. 2, edited by T. J. Ahrens, pp. 269–290, AGU, Washington, D.C., 1995.

Brandeis, G., and C. Jaupart, On the interaction between convection and crystallization in cooling magma chambers, *Earth Planet. Sci. Lett.*, *77*, 345–361, 1986.

Browning, P., The petrology, geochemistry, and structure of the

plutonic rocks of the Oman ophiolite, Ph.D. thesis, Open Univ., Milton Keynes, England, 1982.

Browning, P., Cryptic variation within the Cumulate Sequence of the Oman ophiolite: Magma chamber depth and petrological implications, in *Ophiolites and Oceanic Lithosphere*, pp. 71–82, Geol. Soc. of London, London, 1984.

Browning, P., S. Roberts, and T. Alabaster, Fine-scale modal layering and cyclic units in ultramafic cumulates from the CY-4 Borehole, Troodos Ophiolite; evidence for an open system magma chamber, Cyprus Crustal Study Project, hole CY-4 initial report, pp. 193–220, Geol. Surv. of Can., Ottawa, 1989.

Buening, D. K., and P. R. Buseck, Fe-Mg lattice diffusion in olivine, *J. Geophys. Res.*, *78*, 6852–6862, 1973.

Campbell, I. H., Some problems with the cumulus theory, *Lithos*, *11*, 311–323, 1978.

Cann, J. R., A model for oceanic crustal structure developed, *Geophys. J. R. Astron. Soc.*, *39*, 169–187, 1974.

Caress, D. W., M. S. Burnett, and J. A. Orcutt, Tomographic image of the axial low-velocity zone at 12°50′N on the East Pacific Rise, *J. Geophys. Res.*, *97*, 9243–9263, 1992.

Ceuleneer, G., and M. Rabinowicz, Mantle flow and melt migration beneath oceanic ridges: Models derived from observations in ophiolites, in *Mantle Flow and Melt Generation at Mid-Ocean Ridges, Geophys. Monogr. Ser.*, vol. 71, edited by J. Phipps Morgan, pp. 123–154, AGU, Washington, D.C., 1992.

Ceuleneer, G., M. Monnereau, and I. Amri, Thermal structure of a fossil mantle diapir inferred from the distribution of mafic cumulates, *Nature*, *379*, 149–153, 1996.

Chalokwu, C. I., and N. K. Grant, Reequilibration of olivine with trapped liquid in the Duluth complex, Minnesota, *Geology*, *15*, 71–74, 1987.

Chen, Y., and W. J. Morgan, A nonlinear rheology model for mid-ocean ridge axial topography, *J. Geophys. Res.*, *95*, 17,583–17,604, 1990.

Chen, Y. J., and J. Phipps Morgan, The effects of spreading rate, the magma budget, and the geometry of magma emplacement on the axial heat flux at mid-ocean ridges, *J. Geophys. Res.*, *101*, 11,475–11,482, 1996.

Coleman, R. G., and C. A. Hopson, Introduction to the Oman ophiolite special issue, *J. Geophys. Res.*, *86*, 2495–2496, 1981.

Conrad, M. E., and H. R. Naslund, Modally-graded rhythmic layering in the Skaergaard intrusion, *J. Petrol.*, *30*, 251–269, 1989.

Cox, K. G., J. D. Bell, and R. J. Pankhurst, *The Interpretation of Igneous Rocks*, Allen and Unwin, Winchester, Mass., 1979.

Detrick, R. S., P. Buhl, E. Vera, J. Mutter, J. Orcutt, J. Madsen, and T. Brocher, Multichannel seismic imaging of a crustal magma chamber along the East Pacific Rise, *Nature*, *326*, 35–41, 1987.

Dick, H. J. B., and J. H. Natland, Late-stage melt evolution and transport in the shallow mantle beneath the East Pacific Rise, *Proc. Ocean Drill. Program Sci. Res.*, *147*, 103–134, 1996.

Dowty, E., Crystal growth and nucleation theory and the numerical simulation of igneous crystallization, in *Physics of Magmatic Processes*, edited by R. B. Hargraves, pp. 419–485, Princeton Univ. Press, Princeton, N. J., 1980.

Dunn, R. A., D. R. Toomey, S. C. Solomon, and G. M. Purdy, Seismic structure of the lower crust and Moho beneath the East Pacific Rise at 9°30′N (abstract), *Eos Trans. AGU*, *75*(44), Fall Meet. Suppl., 657, 1994.

Ernewein, M., C. Pflumio, and H. Whitechurch, The death of an accretion zone as evidenced by the magmatic history of the Sumail ophiolite (Oman), *Tectonophysics*, *151*, 247–274, 1988.

Forsyth, D. W., Geophysical constraints on mantle flow and melt generation beneath mid-ocean ridges, in *Mantle Flow and Melt Generation at Mid-Ocean Ridges, Geophys. Monogr. Ser.*, vol. 71, edited by J. Phipps Morgan, pp. 1–65, AGU, Washington, D.C., 1992.

Garmany, J., Accumulations of melt at the base of young oceanic crust, *Nature*, *340*, 628–632, 1989.

Geotimes, Penrose field conference on ophiolites, *17*, 24–25, 1972.

Grove, T. L., and W. B. Bryan, Fractionation of pyroxene-phyric MORB at low pressure: An experimental study, *Contrib. Mineral. Petrol.*, *84*, 293–309, 1983.

Grove, T. L., M. B. Baker, and R. J. Kinzler, Coupled CaAl-NaSi diffusion in plagioclase feldspar: Experiments and applications to cooling rate speedometry, *Goechim. Cosmochim. Acta*, *48*, 2113–2121, 1984.

Grove, T. L., R. J. Kinzler, and W. B. Bryan, Fractionation of mid-ocean ridge basalt (MORB), in *Mantle Flow and Melt Generation at Mid-Ocean Ridges, Geophys. Monogr. Ser.*, edited by J. Phipps Morgan, pp. 281–310, AGU, Washington, D.C., 1992.

Gudmundsson, A., Emplacement of dikes, sills and crustal magma chambers at divergent plate boundaries, *Tectonophysics*, *176*, 257–275, 1990.

Harding, A. J., J. A. Orcutt, M. E. Kappus, E. E. Vera, J. C. Mutter, P. Buhl, R. S. Detrick, and T. M. Brocher, Structure of young oceanic crust at 13°N on the East Pacific Rise from expanding spread profiles, *J. Geophys. Res.*, *94*, 12,163–12,196, 1989.

Hart, S. R., Equilibration during mantle melting: A fractal tree model, *Proc. Natl. Acad. Sci. U.S.A.*, *90*, 11,914–11,918, 1993.

Henstock, T. J., A. W. Woods, and R. S. White, The accretion of oceanic crust by episodic sill intrusion, *J. Geophys. Res.*, *98*, 4143–4161, 1993.

Hirth, G., and D. L. Kohlstedt, Experimental constraints on the dynamics of the partially molten upper mantle: Deformation in the diffusion creep regime, *J. Geophys. Res.*, *100*, 1981–2001, 1995a.

Hirth, G., and D. L. Kohlstedt, Experimental constraints on the dynamics of the partially molten upper mantle, 2, Deformation in the dislocation creep regime, *J. Geophys. Res.*, *100*, 15,441–15,449, 1995b.

Hirth, G., and D. L. Kohlstedt, Water in the oceanic mantle: Implications for rheology, melt extraction, and the evolution of the lithosphere, *Earth Planet. Sci. Lett.*, *144*, 93–108, 1996.

Hofmann, A. W., Diffusion in natural silicate melts: A critical review, in *Physics of Magmatic Processes*, edited by R. B. Hargraves, chap. 9, pp. 385–417, Princeton Univ. Press, Princeton, N. J., 1980.

Hooft, E. E., and R. S. Detrick, The role of density in the accumulation of basaltic melts at mid-ocean ridges, *Geophys. Res. Lett.*, *20*, 423–426, 1993.

Hort, M., B. D. Marsh, and T. Spohn, Igneous layering through oscillatory nucleation and crystal setting in well-mixed magmas, *Contrib. Mineral. Petrol.*, *114*, 425–440, 1993.

Huppert, H. E., and R. S. J. Sparks, Restrictions on the compositions of mid-ocean ridge basalts: A fluid dynamical investigations, *Nature*, *286*, 46–48, 1980.

Huppert, H. E., J. S. Turner, and R. S. J. Sparks, Replenished magma chambers: Effects of compositional zonation and input rates, *Earth Planet. Sci. Lett.*, *57*, 345–357, 1982.

Ildefonse, B., A. Nicolas, and F. Boudier, Evidence from the Oman ophiolite for sudden stress changes during melt injection at oceanic spreading centres, *Nature*, *366*, 673–675, 1993.

Irvine, T. N., Magmatic infiltration metasomatism, double-diffusive fractional crystallization, and adcumulus growth in the Muskox intrusion and other layered intrusions, in *Physics of Magmatic Processes*, edited by R. B. Hargraves, chap. 8, pp. 325–383, Princeton Univ. Press, Princeton, N. J., 1980.

Kelemen, P. B., and E. Aharonov, Periodic formation of magma fractures and generation of layered gabbros in the lower crust beneath oceanic spreading centers, in *Geophysical Monograph Series*, edited by R. Buck, AGU, Washington, D.C., in press, 1997.

Kelemen, P. B., J. A. Whitehead, E. Aharonov, and K. A. Jordahl, Experiments on flow focusing in soluble porous media, with applications to melt extraction from the mantle, *J. Geophys. Res.*, *100*, 475–496, 1995a.

Kelemen, P. B., N. Shimizu, and V. J. M. Salters, Extraction of mid-ocean-ridge basalt from the upwelling mantle by focused flow of melt in dunite channels, *Nature*, *375*, 747–753, 1995b.

Kelemen, P. B., K. Koga, and N. Shimizu, Geochemistry of gabbro sills in the crust/mantle transition zone of the Oman ophiolite: Implications for the origin of the oceanic lower crust, *Earth Planet. Sci. Lett.*, *146*, 475–488, 1997a.

Kelemen, P. B., G. Hirth, N. Shimizu, M. Spiegelman, and H. J. B. Dick, A review of melt migration processes in the adiabatically upwelling mantle beneath oceanic spreading ridges, *Philos. Trans. R. Soc. London A*, *355*, 283–318, 1997b.

Kent, G. M., A. J. Harding, and J. A. Orcutt, Evidence for a smaller magma chamber beneath the East Pacific Rise at 9°30′N, *Nature*, *344*, 650–653, 1990.

Kinzler, R. J., and T. L. Grove, Primary magmas of mid-ocean ridge basalts, 2, Applications, *J. Geophys. Res.*, *97*, 6907–6926, 1992.

Kirkpatrick, R. J., Nucleation and growth of plagioclase, Makaopuhi and Alae lava lakes, *Geol. Soc. Am. Bull.*, *88*, 78–84, 1977.

Korenaga, J., and P. B. Kelemen, Melt migration through the oceanic lower crust: A constraint from melt percolation modeling with finite solid diffusion, *Earth Planet. Sci. Lett.*, in press, 1997.

Koyaguchi, T., M. A. Hallworth, and H. E. Huppert, An experimental study on the effects of phenocrysts on convection in magmas, *J. Volcanol. Geotherm. Res.*, *55*, 15–32, 1993.

Lin, J., and E. M. Parmentier, Mechanisms of lithospheric extension at mid-ocean ridges, *Geophys. J.*, *96*, 1–22, 1989.

Lin, J., and J. Phipps Morgan, The spreading dependence of three-dimensional mid-ocean gravity structure, *Geophys. Res. Lett.*, *19*, 13–16, 1992.

Lippard, S. J., A. W. Shelton, and I. Gass, *The Ophiolite of Northern Oman*, Blackwell, Cambridge, Mass., 1986.

Liu, M., and R. A. Yund, NaSi-CaAl interdiffusion in plagioclase, *Am. Mineral.*, *77*, 275–283, 1992.

Maaløe, S., The origin of rhythmic layering, *Mineral. Mag.*, *42*, 337–345, 1978.

Maaløe, S., Magma accumulation in the ascending mantle, *J. Geol. Soc. London*, *138*, 223–236, 1981.

Macdonald, K. C., Mid-ocean ridges: Fine scale tectonic, volcanic and hydrothermal processes within the plate boundary zone, *Annu. Rev. Earth Planet. Sci.*, *10*, 155–190, 1982.

McBirney, A. R., Further considerations of double-diffusive stratification and layering in the Skaergaard intrusion, *J. Petrol.*, *26*, 993–1985, 1985.

McBirney, A. R., *Igneous Petrology*, 2nd ed., Jones and Bartlett, Boston, Mass., 1993.

McBirney, A. R., and R. M. Noyes, Crystallization and layering of the Skaergaard intrusion, *J. Petrol.*, *20*, 487–554, 1979.

McKenzie, D., The generation and compaction of partially molten rock, *J. Petrol.*, *25*, 713–765, 1984.

McKenzie, D., Some remarks on the movement of small melt fractions in the mantle, *Earth Planet. Sci. Lett.*, *95*, 53–72, 1989.

Meyer, P. S., H. J. B. Dick, and G. Thompson, Cumulate gabbros from the Southwest Indian Ridge, 54°S-7°16′E: Implications for magmatic processes at a slow spreading ridge, *Contrib. Mineral. Petrol.*, *103*, 44–63, 1989.

Michard, A., F. Boudier, and B. Goffe, Obduction versus subduction and collision in the Oman case and other Tethyan settings, in *Ophiolite Genesis and Evolution of the Oceanic Lithosphere*, pp. 447–467, Kluwer Acad., Boston, Mass., 1991.

Mo, X., I. S. E. Carmichael, M. Rivers, and J. Stebbins, Partial molar volume of Fe_2O_3 in multicomponent silicate liquids and the pressure dependence of oxygen fugacity in magmas, *Mineral. Mag.*, *45*, 237–245, 1982.

Montigny, R., O. Le Mer, R. Thuizat, and H. Whitechurch, K-Ar and $^{40}Ar/^{39}Ar$ study of metamorphic rocks associated with the Oman ophiolite: Tectonic implication, *Tectonophysics*, *151*, 345–362, 1988.

Morse, S. A., Kiglapait geochemistry, I, Systematics, sampling, and density, *J. Petrol.*, *20*, 555–590, 1979.

Nelson, S. A., and I. S. E. Carmichael, Partial molar volume of oxide components in silicate liquids, *Contrib. Mineral. Petrol.*, *71*, 117–124, 1979.

Nicolas, A., A melt extraction model based on structural studies in mantle peridotites, *J. Petrol.*, *27*, 999–1022, 1986.

Nicolas, A., Kinematics in magmatic rocks, *J. Petrol.*, *33*, 891–915, 1988.

Nicolas, A., *Structures of Ophiolites and Dynamics of Oceanic Lithosphere*, 367 pp., Kluwer Acad., Norwell, Mass., 1989.

Nicolas, A., Melt extraction from mantle peridotites: Hydrofracturing and porous flow, with consequences for oceanic ridge activity, in *Magma Transport and Storage*, edited by M. P. Ryan, pp. 159–174, John Wiley, New York, 1990.

Nicolas, A., and F. Boudier, Mapping oceanic ridge segments in Oman ophiolite, *J. Geophys. Res.*, *100*, 6179–6197, 1995.

Nicolas, A., and A. Prinzhofer, Cumulative or residual origin for the transition zone in ophiolites: Structural evidence, *J. Petrol.*, *24*, 188–206, 1983.

Nicolas, A., I. Reuber, and K. Benn, A new magma chamber model based on structural studies in the Oman ophiolite, *Tectonophysics*, *151*, 87–105, 1988.

Nicolas, A., C. Fraydier, M. Godard, and A. Vauchez, Magma chambers at oceanic ridges: How large?, *Geology*, *21*, 53–56, 1993.

Nicolas, A., B. Ildefonse, and F. Boudier, Flow mechanism and viscosity in basaltic magma chambers, *Geophys. Res. Lett.*, *23*, 2013–2016, 1996.

O'Hara, M. J., and R. E. Matthews, Geochemical evolution in an advancing periodically replenished, periodically tapped, continuously fractionated magma chamber, *J. Geol. Soc. London*, *138*, 237–277, 1981.

Pallister, J. S., Parent magmas of the Samail ophiolite, Oman, in *Ophiolites and Oceanic Lithosphere*, pp. 63–70, Geol. Soc. of London, London, 1984.

Pallister, J. S., and C. A. Hopson, Samail ophiolite plutonic suite: Field relations, phase variation, cryptic variation and layering, and a model of a spreading ridge magma chamber, *J. Geophys. Res.*, *86*, 2593–2644, 1981.

Pallister, J. S., and R. J. Knight, Rare-earth element geochemistry of the Samail Ophiolite near Ibra, Oman, *J. Geophys. Res.*, *86*, 2673–2697, 1981.

Panjasawatwong, Y., L. V. Danyushevsky, A. J. Crawford, and K. L. Harris, An experimental study of the effects of melt composition on plagioclase - melt equilibria at 5 and 10 kbar: Implications for the origin of magmatic high-An plagioclase, *Contrib. Mineral. Petrol.*, *118*, 420–432, 1995.

Pearce, J. A., T. Alabaster, A. W. Shelton, and M. P. Searle, The Oman ophiolite as a Cretaceous arc-basin complex: Evidence and implications, *Philos. Trans. R. Soc. London, Ser. A*, *300*, 299–317, 1981.

Phipps Morgan, J., and Y. J. Chen, The genesis of oceanic crust: Magma injection, hydrothermal circulation, and crustal flow, *J. Geophys. Res.*, *98*, 6283–6297, 1993.

Phipps Morgan, J., A. Harding, J. Orcutt, G. Kent, and Y. J. Chen, An observational and theoretical synthesis of magma chamber geometry and crustal genesis along a mid-ocean ridge spreading center, in *Magmatic Systems*, edited by M. P. Ryan, pp. 139–178, Academic, San Diego, Calif., 1994.

Quick, J. E., and R. P. Denlinger, Ductile deformation and the origin of layered gabbro in ophiolites, *J. Geophys. Res.*, *98*, 14,015–14,027, 1993.

Rabinowicz, M., G. Ceuleneer, and A. Nicolas, Melt segregation and flow in mantle diapirs below spreading centers: Evidence from the Oman ophiolite, *J. Geophys. Res.*, *92*, 3475–3486, 1987.

Rubin, A., A comparison of rift-zone tectonics in Iceland and Hawaii, *Bull. Volcanol.*, *52*, 302–319, 1990.

Shimizu, N., and S. R. Hart, Application of the ion microprobe to geochemistry and cosmochemistry, *Annu. Rev. Earth Planet. Sci.*, *10*, 483–526, 1982.

Sinton, J. M., and R. S. Detrick, Mid-ocean ridge magma chambers, *J. Geophys. Res.*, *97*, 197–216, 1992.

Sisson, T. W., and T. L. Grove, Temperatures and H_2O contents

of low-MgO high-alumina basalts, *Contrib. Mineral. Petrol.*, *113*, 167–184, 1993.

Smewing, J. D., Mixing characteristics and compositional differences in mantle-derived melts beneath spreading axes: Evidence from cyclically layered rocks in the ophiolite of North Oman, *J. Geophys. Res.*, *86*, 2645–2659, 1981.

Sneeringer, M., S. R. Hart, and N. Shimizu, Strontium and samarium diffusion in diopside, *Geochim. Cosmochim. Acta*, *48*, 1589–1608, 1984.

Sparks, R. S. J., and H. E. Huppert, Density changes during the fractional crystallization of basaltic magmas: Fluid dynamic implications, *Contrib. Mineral. Petrol.*, *85*, 300–309, 1984.

Sparks, R. S. J., H. E. Huppert, R. C. Kerr, D. P. McKenzie, and S. R. Tait, Postcumulus processes in layered intrusions, *Geol. Mag.*, *122*, 555–568, 1985.

Sparks, R. S. J., H. E. Huppert, T. Koyaguchi, and M. A. Hallworth, Origin of modal and rhythmic igneous layering by sedimentation in a convecting magma chamber, *Nature*, *361*, 246–249, 1993.

Spiegelman, M., Physics of melt extraction: Theory, implications and applications, *Philos. Trans. R. Soc. London, Ser. A*, *342*, 23–41, 1993.

Streckeisen, A., To each plutonic rock its proper name, *Earth Sci. Rev.*, *12*, 1–33, 1976.

Tilton, G. R., C. A. Hopson, and J. E. Wright, Uranium-lead isotopic ages of the Samail ophiolite, *J. Geophys. Res.*, *86*, 2763–2775, 1981.

Toomey, D. R., G. M. Purdy, S. C. Solomon, and W. S. D. Wilcock, The three-dimensional seismic velocity structure of the East Pacific Rise near latitude 9°30′N, *Nature*, *347*, 639–645, 1990.

Turner, J. S., and C. F. Chen, Two-dimensional effects in double-diffusive convection, *J. Fluid Mech.*, *63*, 577–592, 1974.

Van der Molen, I., and M. S. Paterson, Experimental deformation of partially-melted granite, *Contrib. Mineral. Petrol.*, *70*, 299–318, 1979.

Vera, E. E., J. C. Mutter, P. Buhl, J. A. Orcutt, A. J. Harding, M. E. Kappus, R. S. Detrick, and T. M. Brocher, The structure of 0- to 0.2-m.y.-old oceanic crust at 9°N on the East Pacific Rise from expanded spread profiles, *J. Geophys. Res.*, *95*, 15,529–15,556, 1990.

Wager, L. R., Differing powers of crystal nucleation as a factor producing diversity in layered igneous intrusions, *Geol. Mag.*, *96*, 75–80, 1969.

Wager, L. R., and G. M. Brown, *Layered Igneous Rocks*, Oliver and Boyd, White Plains, N. Y., 1968.

Walker, D., T. Shibata, and S. E. DeLong, Abyssal tholeiites from the Oceanographer fracture zone, *Contrib. Mineral. Petrol.*, *114*, 477–489, 1979.

Wickham, S. M., The segregation and emplacement of granitic magmas, *J. Geol. Soc. London*, *144*, 281–297, 1987.

Wilcock, W. S. D., S. C. Solomon, G. M. Purdy, and D. R. Toomey, The seismic attenuation structure of a fast-spreading mid-ocean ridge, *Science*, *258*, 1470–1474, 1992.

Yang, H. J., R. J. Kinzler, and T. L. Grove, Experiments and models of anhydrous, basaltic olivine-plagioclase-augite saturated melts from 0.001 to 10 kbar, *Contrib. Mineral. Petrol.*, *124*, 1–18, 1996.

P. B. Kelemen and J. Korenaga, Department of Geology and Geophysics, Woods Hole Oceanographic Institution, Woods Hole, MA 02543-1542. (e-mail: pkelemen@whoi.edu; korenaga@mit.edu)

(Received January 30, 1997; revised September 4, 1997; accepted September 11, 1997.)